THE ASTROPHYSICAL JOURNAL, 365:704–728, 1990 December 20

EINSTEIN OBSERVATORY CORONAL TEMPERATURES OF LATE-TYPE STARS

J. H. M. M. SCHMITT
Max-Planck-Institut für Physik und Astrophysik, Institut für Extraterrestrische Physik

A. COLLURA
IAIF-CNR Palermo

S. SCIORTINO AND G. S. VAIANA
Osservatorio Astronomica di Palermo

F. R. HARNDEN, JR.
Harvard-Smithsonian Center for Astrophysics

AND

R. ROSNER
Department of Astronomy and Astrophysics, and Enrico Fermi Institute, The University of Chicago
Received 1990 April 6; accepted 1990 June 15

ABSTRACT

We present the results of an extensive survey of coronal temperatures of late-type stars using the *Einstein Observatory* Imaging Proportional Counter and discuss various biases that may arise during the process of determining X-ray temperatures from low-resolution, broad-band data. From the Bright Star Catalog and its Supplement and the Woolley Catalog, we derive a sample consisting of 130 late-type stars which were observed with sufficiently high signal-to-noise ratio and whose $B-V$ colors are redder than 0.0. Our spectral analysis shows that the frequently found one- and two-temperature descriptions are largely influenced by the signal-to-noise ratio of the data, and that models employing continuous emission measure distributions can provide equally adequate and physically more meaningful and more plausible descriptions.

For four groups of stars (main-sequence F and G stars, main-sequence M stars, yellow giants, and RS CVn systems), we find intrinsic differences in their differential emission measure distributions. In general, M dwarfs—whenever observed with sufficient signal-to-noise ratio—show evidence for high-temperature gas ($T > 10^7$ K) in conjunction with lower temperature ($T \sim 3 \times 10^6$ K) material, while main-sequence stars of spectral type F and G have the high-temperature component either absent or very weak. For the majority of the giant stars we studied (all of which have X-ray luminosities above the median for this class), there is evidence of very hot coronae ($T > 10^7$ K), but without the lower temperature component which appears in the dwarf stars. As a group, RS CVn systems also show evidence for extremely hot coronae ($T > 10^{7.5}$ K), sometimes with no accompanying lower temperature material; in this sense, they resemble the behavior of the giants, but with significantly higher coronal temperatures.

Subject headings: stars: coronae — stars: late-type — stars: X-rays

I. INTRODUCTION

X-ray data obtained with the *Einstein Observatory* (cf. Giacconi *et al.* 1979) have brought about a major change in our perception of stellar coronae as a result of the observation of X-ray emission from normal stars throughout the H-R diagram. The presence of coronae, and the operation of associated nonradiative heating mechanisms, have been shown to be the rule rather than the exception (see Vaiana *et al.* 1981; Rosner, Golub, and Vaiana 1985; Linsky 1985; and references therein).

Previously undertaken X-ray surveys have concentrated on the problem of establishing the *levels* of stellar X-ray emission as a function of stellar properties. Typically, this has involved the construction of (maximum likelihood) X-ray luminosity distribution functions from optically selected samples of stars such as M stars (Rosner *et al.* 1981), G stars (Maggio *et al.* 1987), F stars (Schmitt *et al.* 1985*a*), the Hyades stars (Micela *et al.* 1988), and the Pleiades stars (Micela *et al.* 1990). Detailed studies of the physical properties characterizing the plasmas responsible for stellar X-ray emission have tended to concentrate on rather small, isolated samples of stars; and only in a few cases were attempts made to systematically consider a homogeneous class of objects (cf. Stern, Antiochos, and Harnden 1986 for a spectral study of the Hyades stars; and Schmitt *et al.* 1987 for a comparison between observations of 11 stars observed with both the *Einstein* and the *EXOSAT* satellites). Nevertheless, these studies have led to the recognition that such plasmas can have several temperature components, that there is a dependence of the photon spectrum on the activity of the star, and that there may be a correlation between X-ray luminosity and temperature (Vaiana 1983; Schmitt *et al.* 1985*a*; Stern, Antiochos, and Harnden 1986; Schmitt *et al.* 1987).

The analysis and interpretation of *Einstein* stellar X-ray spectra as a whole has heretofore not been attempted: the basic goal of this paper is to carry out this task and present a survey of the coronal X-ray temperatures of late-type stars as observed with the *Einstein* Imaging Proportional Counter (IPC; cf. Gorenstein, Harnden, and Fabricant 1981), thereby exploring the physical parameters of stellar coronae throughout the H-R diagram.

The IPC, with its rather moderate energy resolution ($\Delta E/E \sim 1$), is limited in its ability to deduce definitive coronal parameters of complex source spectra. Unfortunately, data

with higher spectral resolution are available only for an exceedingly small number of sources. Only two sources—Capella, the strongest coronal X-ray source, and the RS CVn system σ CrB—were observed with the *Einstein* Focal Plane Crystal Spectrometer (FPCS; $E/\Delta E \sim 100$; cf. Vedder and Canizares 1983; Agrawal, Markert, and Riegler 1985), and Capella was the only coronal source observed with the *Einstein* Objective Grating Spectrometer (OGS; $E/\Delta E \sim 40$; cf. Mewe *et al.* 1982). The *Einstein* Solid State Spectrometer (SSS) obtained spectra of about eight RS CVn systems, two M dwarfs, and one G dwarf with an energy resolution $E/\Delta E \sim 10$ (Swank 1984). Finally, the *EXOSAT* transmission grating ($E/\Delta E \sim 50$) was used to observe X-ray spectra of Capella, σ CrB, and Procyon (Schrijver 1985), and covered the important wavelength range between 90 and 140 Å. While these higher resolution observations are extremely interesting, their number is simply too small to characterize the general spectral properties of X-ray emission throughout the H-R diagram, and hence for the time being we must rely upon the lower spectral resolution IPC measurements. However, we shall call upon the higher resolution data whenever needed in our discussions.

Given the IPC's limitations in spectral resolution, as well as the rather low signal-to-noise ratios encountered in many of the IPC observations, particular care is required in order to interpret the IPC data in a physically meaningful way. For these reasons, we discuss in detail our spectral fitting procedures and examine possible biases and selection effects which may result from our procedures. We also treat the problem of nonuniqueness of spectral parameters that arises when differing spectral models are employed.

The detailed plan of our paper is as follows: in § II we describe the construction of our sample and the observations which pertain to it. Our procedures for the spectral analysis of low-resolution IPC X-ray data and the physics underlying coronal X-ray emission are briefly discussed in § III, and the results of our temperature analyses are presented in § IV. We summarize our conclusions in the final section and, in three appendices, elaborate some details regarding instrument characteristics, the technicalities of the fitting procedures, and simulations carried out to substantiate the reliability of our results.

II. SAMPLE STARS AND OBSERVATIONS

We constructed our sample by first compiling a list of all X-ray sources which were detected with *Einstein Observatory* IPC as pointed or serendipitous targets and which could be identified with an entry in the Bright Star Catalog (Hoffleit and Jaschek 1982, hereafter BSC), its Supplement (Hoffleit Saladyga, and Wlasuk 1984), or the Woolley Catalog (Woolley *et al.* 1970). We then added the RS CVn systems studied by Majer *et al.* (1986) to the list in order to facilitate a comparison between the various groups of stars. Finally, we eliminated those sources which contained less than 200 counts in their X-ray spectra or whose spectra might have been perturbed by proximity to the detector edges or to the entrance window support structure (cf. Appendix A of Micela *et al.* 1988). These selection criteria, while providing a sample of well-studied objects with sufficiently high signal-to-noise ratio to allow meaningful X-ray spectral studies, do not ensure sample homogeneity and lack of bias. Indeed, the Bright Star Catalog provides a subsample of magnitude-limited objects, the objects selected from the Woolley Catalog are distance-limited, and our entire sample is "pseudo"–X-ray flux–limited as a result of the imposition of an X-ray counts limit on this set of observations which have rather similar exposure times. For these reasons, extrapolation of our results to stars as a whole must be done with considerable care; in fact, extrapolation of the fainter X-ray stars may be unwarranted.

For identification of an X-ray source with a cataloged object, we required the X-ray and optical position to match to better than 2′. We considered only stars with $B-V > 0$ in order to restrict the analysis to late-type stars, of spectral type A, F, G, K, and M. However, none of the few early A stars detected in X-rays by the *Einstein Observatory* meets the selection criteria for inclusion in our sample.

Based on the information provided in the catalogs, we classified the sample stars as single, binary, RS CVn, and ambiguous. We classified all objects as binaries in which two or more objects are expected to contribute significantly to the total (spatially unresolved) X-ray emission; however, binaries containing an A-type star, or containing a cool white dwarf (e.g., Procyon), or binaries where High Resolution Imager (Giacconi *et al.* 1979) observations showed the X-ray emission to come predominantly from one of the components, were classified as single stars. The single and binary stars were further subdivided into luminosity classes; in the case of binaries, the luminosity class refers to that of the primary component. The restriction to stars cataloged in the Bright Star Catalog or Woolley Catalog may seem overly restrictive, and in fact many X-ray sources can be identified with fainter stellar optical counterparts. However, because we have decided to focus on a well-defined sample in both the optical and X-rays, the relative lack of further information on distance, color, spectral type, and binarity for these fainter counterparts has led us to exclude them from this study.

In Table 1 we list our sample stars drawn from the Bright Star Catalog, the Bright Star Catalog Supplement, and the Woolley Catalog, together with the requisite optical, X-ray, and other needed information for each star. We note in passing that stars found in both the Bright Star Catalog and Woolley Catalog are referred to as BSC objects, and that whenever color information was not available in the Woolley Catalog we computed a color using the absolute magnitude and the relation given by Pettersen (1982). In the first column of Table 1 we provide a cross-reference number (indicated in the text as a bracketed number following star names) intended solely to aid the reader in locating the Table 1 entry for objects from subsequent tables; column (2) contains star names (note that the four, signed-numeric entries are BD numbers). The table also provides the following additional information: identifying numbers (cols. [3]–[5]), IPC sequence number and source number (cols. [6]–[7]), total number of counts in the X-ray spectrum (col. [8]), $B-V$ and spectral type (cols. [9] and [10]), and distance (col. [11]). Our categorization of the stars as single (S), binary (B), RS CVn (R, for "classical" members, or dR, for members not known to contain a giant), or ambiguous (A) is indicated as "Category" in column (12), and in the final column, we summarize the results of fitting the X-ray spectra with various coronal models, defining a "fit code" according to the scheme discussed in § IV*d* (cf. Table 6).

Our full sample consists of 165 different observations of 130 distinct objects: 82 are taken from the Bright Star Catalog, 18 taken from its supplement or the complete list of *Einstein* observations of RS CVn systems, and 30 from the Woolley Catalog. Of the 130 stars, 48 are main-sequence stars with $B-V$ color index <1, 26 are main-sequence stars with

TABLE 1

SAMPLE STARS AND IDENTIFICATIONS

Xref number (1)	Star Name (2)	HR number (3)	HD number (4)	Woolley number (5)	Sequence number (6)	Source number (7)	Counts (8)	B-V (9)	Spectral type (10)	Dist. (pc) (11)	Category (12)	Fit code (13)
1	UV Cet	.....	.....	65	905	7	866	.....	M4EV+M6EV	3	B	2EC
1		.....	.....	65	906	3	373					2EC
1		.....	.....	65	6952	5	1801					U
1		.....	.....	65	6953	4	1896					2EC
2	CC Eri	.....	16157	103	2302	1	690	1.39	K7EV	11	B	A
3	.....	.....	.....	182	7359	1	200	1.36	M1EV	15	S	A
3		.....	.....	182	7360	1	551					2EC
3		.....	.....	182	7361	1	556					A
4	OU Gem	.....	45088	233	5484	2	650	0.93	K3 V	12	B	2EC
5	Ross 614	.....	.....	234	5485	3	527	1.74	M4EV	4	B	A
6	Ross 986	.....	.....	268	5493	4	210	1.71	M5EV	6	A	A
7	YY Gem	.....	60178	278	838	1	1711	1.49	M0EV	15	B	2EC
7		.....	60178	278	2308	1	1394					2C
8	YZ CMi	.....	.....	285	907	1	2566	1.59	M4EV	6	S	2EC
8		.....	.....	285	908	3	1884					2C
8		.....	.....	285	3048	6	3724					2EC
8		.....	.....	285	10640	2	3577					2EC
9	+50 1725	.....	88230	380	4414	2	448	1.38	K7 V	5	S	A
10	AD Leo	.....	.....	388	913	1	33280	1.54	M4EV	5	S	U
11	.....	.....	.....	394	5527	2	212	1.36	K7 V	11	S	A
12	DT Vir	.....	.....	494	5990	1	1007	1.43	M2EV	14	S	2EC
13	EQ Vir	.....	118100	517	917	4	1321	1.18	K5EV	16	S	2EC
13		.....	118100	517	6969	5	1574					2EC
14	Prox Cen	.....	.....	551	3243	3	5006	1.88	M5EV	1	S	2EC
14		.....	.....	551	7689	3	5295					2EC
15	+16 2708	.....	.....	569	5991	2	248	1.48	M0EV	10	S	A
16	Wolf 630	.....	152751	644	3112	1	2460	1.62	M3EV+M4E	6	B	U
17	Ross 867	.....	.....	669	3091	1	402	1.55	M4EV+M5E	11	B	A
18	BY Dra	.....	234677	719	927	1	5944	1.23	M0EV	16	B	2EC
19	Ross 154	.....	.....	729	10311	2	1043	1.73	M4EV	3	S	2EC
20	.....	.....	.....	735	10312	2	1930	1.75	M2EV	11	S	2EC
21	AU Mic	.....	197481	803	2314	1	4190	1.44	M0EV	9	S	2C
22	.....	.....	.....	812	7416	7	224	1.49	M4EV+C VI	15	S	A
23	−21 6267	.....	214479	867	7380	2	1692	1.48	M2EV+M4EV	9	B	2EC
23		.....	214479	867	7381	2	2032					2EC
23		.....	214479	867	7382	1	1551					2EC
24	EQ Peg	.....	.....	896	933	1	2224	1.56	M4EV+M6EV	6	B	2EC
24		.....	.....	896	6972	1	5175					2EC
24		.....	.....	896	6973	2	3823					2EC
25	TZ Ari	.....	.....	9066	7710	2	244	1.82	M5EV	5	S	A
26	VY Ari	.....	17433	9102	7748	3	5532	1.09	G9	21	R	2
27	V371 Ori	.....	.....	9183	7471	2	534	1.52	M3EV	15	S	A

TABLE 1—*Continued*

Xref number (1)	Star Name (2)	HR number (3)	HD number (4)	Woolley number (5)	Sequence number (6)	Source number (7)	Counts (8)	B-V (9)	Spectral type (10)	Dist. (pc) (11)	Category (12)	Fit code (13)
28	+55 1823	.....	.....	9552	7749	5	1508	1.46	M1EV	21	S	2C
29	VW Cep	.....	197433	9703	3365	4	8548	0.86	K0 V	23	B	2EC
30	GT Peg	.....	.....	9799	7362	1	748	1.41	M3EV	23	S	A
30	.....	.....	.....	9799	7363	2	527					2EC
30	.....	.....	.....	9799	7364	1	325					A
31	.....	8	166	.....	2225	1	208	0.75	K0V	15	S	A
32	9 Cet	88	1835	9012	7958	6	375	0.66	G2V	20	S	A
33	β Cet	188	4128	31	4452	4	1531	1.02	K0IIICH-1H K-0.5	16	S	A+
34	ζ And	215	4502	.....	3191	1	1079	1.12	K1IIe	27	R	1-
34		215	4502	.....	3534	3	1695					A-
35	39 Cet	373	7672	.....	3192	1	3040	0.90	G5IIIe	70	R	A-
36	UV Psc	.....	7700	.....	2300	2	410	0.80	.....	125	dR	A-
37	ρ Psc	413	8723	.....	6080	4	290	0.39	F2V:v	26	S	A
38	α Tri	544	11443	9062	845	2	595	0.49	F6IV	18	B	A
39	6 Tri	642	13480	.....	3533	2	670	0.78	G5III+F5V	85	B	12-
40	RZ Cas	815	17138	.....	7737	4	523	0.18	A3V	96	B	A+
41	τ^1 Eri	818	17206	111	5448	4	218	0.48	F6V	14	B	A
42	.....	857	17925	117	9065	3	690	0.87	K2V	8	S	2EC
43	UX Ari	.....	21242	.....	9041	1	14036	0.91	G5IV/V + K0IV	45	R	A+
43		.....	21242	.....	9042	1	11408					12
43		.....	21242	.....	9967	1	8954					2C
44	ϵ Eri	1084	22049	144	3106	1	837	0.88	K2V	3	B	2C
45	.....	1089	22211	.....	8397	7	408	0.63	G0	.....	A	1-
46	V711 Tau	1099	22468	.....	2306	1	7783	0.92	G9V	31	R	A+
46		1099	22468	.....	3152	2	74303					U
46		1099	22468	.....	4496	1	9015					A-
46		1099	22468	.....	5455	1	21145					U
47	39 Tau	1262	25680	160	7918	6	303	0.62	G5V	16	S	A
48	V774 Tau	1322	26923	.....	7606	2	936	0.59	G0IV	50	S	2EC
49	40 Eri	1325	26965	166	865	3	797	0.82	K1V	5	S	2EC
50	.....	.....	27691	.....	9002	5	539	0.56	F8IV	32	A	A
51	71 Tau	1394	28052	.....	9004	6	2822	0.25	F0V	40	B	2EC
52	θ^1 Tau	1411	28307	.....	3512	2	243	0.95	K0IIIbFe-0.5	40	B	A
52		1411	28307	.....	9005	5	1362					2C
53	.....	.....	28363	.....	9005	9	281	0.53	F7V+G0V	59	A	A
54	.....	.....	28568	.....	9006	7	707	0.43	F5V	40	S	2EC
55	.....	1436	28736	.....	350	1	293	0.42	F5V	40	S	A
56	.....	1442	28867	.....	10538	8	261	0.07	B9IVn	150	B	A-
57	3 Cam	1467	29317	.....	4942	3	231	1.07	K0III	85	B	A
58	RZ Eri	.....	30050	.....	3195	2	510	0.67	.....	105	R	1-
59	12 Cam	.....	32357	.....	3196	1	389	1.12	.....	134	dR	A-

TABLE 1—*Continued*

Xref number (1)	Star Name (2)	HR number (3)	HD number (4)	Woolley number (5)	Sequence number (6)	Source number (7)	Counts (8)	B-V (9)	Spectral type (10)	Dist. (pc) (11)	Category (12)	Fit code (13)
60	β Eri	1666	33111	9175	5471	4	445	0.13	A3III	20	S	A
61	Capella	1708	34029	194	849	1	8165	0.80	G5IIIe+G0III	13	R	2C
62	111 Tau	1780	35296	202	4348	3	400	0.53	F8V	15	S	A
63	ν^2 Col	1935	37495	9186	3720	5	754	0.46	F4V	21	S	A
64	χ^1 Ori	2047	39587	222	4347	2	586	0.59	G0V	10	B	2EC
65	α Car	2326	45348	.....	847	4	297	0.15	F0II	36	S	A-
65		2326	45348	.....	6960	6	2730					12-
66	63 Gem	2846	58728	.....	9692	3	778	0.39	F5V+F5V	31	B	A
67	α CMi	2943	61421	280	848	4	3548	0.42	F5IV-V	3	S	A-
68	σ Gem	2973	62044	.....	2310	1	3185	1.12	K1III	59	R	A-
68		2973	62044	.....	2311	1	5226					A
69	AE Lyn	3119	65626	.....	5184	3	1135	0.62	F8V	26	dR	A+
70	α Cha	3318	71243	305	10100	2	241	0.39	F5III	19	S	A
71	π^1 UMa	3391	72905	311	501	3	327	0.62	G1.5Vb	14	S	A
71		3391	72905	.....	6964	6	2980					2C
72	RZ Cnc	.....	73343	.....	3204	2	331	1.18	.....	310	R	1-
73	.....	.....	75767	.....	5185	4	217	0.64	dG1	28	B	A
74	.....	3538	76151	327	7954	4	398	0.67	G3V	12	S	A
75	24 UMa	3771	82210	.....	3535	1	1283	0.77	G4III-IV	24	S	A
76	ν^1 Hya	3903	85444	.....	7607	4	460	0.92	G7-III-IIIb	50	S	A
77	μ Vel	4216	93497	.....	4448	1	1256	0.90	G5III+G2V	30	B	A
78	ξ UMa	4374	98230	423	5189	1	2878	0.59	G0V	7	R	2C
79	61 UMa	4496	101501	434	3530	2	311	0.72	G8V	8	S	A
80	93 Leo	4527	102509	.....	5190	2	715	0.55	A7V+G5III-IV e	45	R	A+
81	α Crv	4623	105452	9389	5538	2	258	0.32	F2III-IV	14	S	A
82	DK Dra	4665	106677	.....	3208	2	1311	1.14	K0III	140	R	A-
83	AS Dra	.....	107760	.....	3209	1	207	0.73	.....	31	dR	A
84	.....	4867	111456	9417	7913	2	699	0.46	F5V	24	S	A+
85	RS CVn	.....	114519	9430	3211	3	1091	0.67	.....	145	R	A-
86	β Com	4983	114710	502	4457	1	251	0.57	G0V	8	S	A
87	59 Vir	5011	115383	504	3531	2	323	0.59	G0Vs	13	S	A
88	BH CVn	5110	118216	.....	3213	4	5773	0.40	F2IV	45	R	A+
89	τ Boo	5185	120136	527	5549	2	445	0.48	F6IV	17	B	A
90	18 Boo	5365	125451	.....	9705	1	233	0.38	F5IV	46	S	A
91	θ Boo	5404	126660	549	5559	7	2458	0.50	F7V	14	A	A+
92	α Cen	5459	128620	559	4436	2	10225	0.88	G2V	1	S	U
93	ν Vir	5487	129502	9491	5564	5	940	0.38	F2III	22	B	U
94	ξ Boo	5544	131156	566	4146	4	715	0.76	G8V+K4V	6	R	12E
94		5544	131156	566	10418	1	1654					2EC
95	44 Boo	5618	133640	575	3366	1	7092	0.65	F9-G1Vn	12	B	2EC
96	λ Ser	5868	141004	598	5576	1	209	0.60	G0V	11	B	A

TABLE 1—*Continued*

Xref number (1)	Star Name (2)	HR number (3)	HD number (4)	Woolley number (5)	Sequence number (6)	Source number (7)	Counts (8)	B-V (9)	Spectral type (10)	Dist. (pc) (11)	Category (12)	Fit code (13)
97	δ CrB	5889	141714	.....	7609	4	1458	0.80	G3.5III-IVFe-1	40	S	A+
98	θ Dra	5986	144284	9538	5191	2	390	0.52	F8IV	20	B	A
99	κ Her	6008	145001	.....	7610	3	480	0.95	G8III	90	S	A-
100	σ CrB	6063	146361	9550	3219	1	5138	0.51	G0VCaIIe	22	dR	A
101	β Her	6148	148856	.....	5584	4	215	0.94	G7IIIa	35	B	A+
102	.....	6349	154417	9583	5992	2	209	0.58	F8.5IV-V	22	S	A+
103	μ Dra	6370	154906	9584	3811	2	308	0.48	F7V	22	B	A
103		6370	154906	9584	7663	1	206					A
104	χ Ser	6561	159876	.....	5605	2	1163	0.26	F0IVδSct	30	B	2EC
105	ω Dra	6596	160922	.....	7888	4	255	0.43	F5V	22	B	A
106	.....	6638	162076	.....	7611	6	1133	0.94	G5IV	110	S	A+
107	Z Her	.....	163930	.....	6970	7	2523	0.59	.....	85	R	1-
108	70 Oph	6752	165341	702	3113	2	1093	0.86	K0V	5	B	A
109	V772 Her	.....	165590	.....	10433	3	16460	0.66	G0V+G8V	30	R	U
110	110 Her	7061	173667	9635	5621	2	1140	0.46	F6V	19	S	A
111	V1762 Cyg	7275	179094	.....	3227	1	1556	1.09	K1IV	48	R	A
111		7275	179094	.....	4948	1	1641					12-
112	α Aql	7557	187642	768	844	9	265	0.22	A7V	5	S	A-
113	.....	7683	190771	9685	5993	1	204	0.65	G5IV	24	S	A
114	β Del	7882	196524	.....	5640	1	663	0.44	F5IV	36	B	A
115	α Equ	8131	202447	.....	5645	4	808	0.53	G0III+A5V	48	S	A
116	ι Cap	8167	203387	.....	3536	1	475	0.90	G8III	40	S	A
117	AD Cap	.....	206046	.....	3229	1	210	1.00	.....	250	R	A-
118	HN Peg	8314	206860	9751	7605	6	1522	0.59	G0V	15	S	2EC
119	ϵ Ind	8387	209100	845	5652	5	359	1.06	K4-5V	3	S	A
120	RT Lac	.....	209318	.....	3153	6	1946	1.14	.....	205	R	1-
121	16 Cep	8400	209369	.....	9711	1	216	0.44	F5V	25	S	A
122	HK Lac	.....	209813	.....	3230	2	297	1.08	K0III+F1V	150	R	A-
123	AR Lac	8448	210334	.....	5011	1	8389	0.72	G2IV+K0III	47	R	1-
123		8448	210334	.....	5012	3	14211					2C
123		8448	210334	.....	5013	3	8453					2C
123		8448	210334	.....	5014	3	7632					1
123		8448	210334	.....	5015	1	3523					A+
123		8448	210334	.....	5016	1	2777					A
124	V350 Lac	8575	213389	.....	3231	3	237	1.15	K2III	69	R	A-
125	IM Peg	8703	216489	.....	3233	1	1395	1.12	K1-2II-IIIe	50	R	1-
126	56 Peg	8796	218356	.....	4233	3	360	1.34	G8Ib	200	A	1-
127	SZ Psc	.....	219113	.....	3234	1	3292	0.84	.....	100	R	1-
128	ν Peg	8905	220657	.....	8396	7	1274	0.61	F8III	28	S	A-
129	λ And	8961	222107	9832	3235	2	5067	1.01	G8III-IV	20	R	A
130	II Peg	.....	224085	.....	3236	1	2836	1.01	.....	29	dR	A+

$B - V \geq 1$, 18 are giants, 32 are RS CVn systems, and six have not been classified for lack of information; this last group also includes objects that could in principle be classified but for which some of the information used in the following work was not available.

For objects observed more than once, the tables of fit results contain individual entries for each data set, but the figures (except as noted below and in the captions) show results only for the *single* data set with the largest number of counts (cf. Table 1) in the X-ray spectrum of each multiply observed object. Hence, different symbols in (most of) the figures correspond to different objects.

III. DATA ANALYSIS AND MODEL CORONAE

a) Spectral Analysis of Low-Resolution X-Ray Data

It is well known that the physical interpretation of many types of spectral data, and especially of low-resolution X-ray data, requires *a priori* assumptions about the form of the incident spectrum and, by inference, the physical processes responsible for the emission. In the case of stars, we have an advantage because the higher resolution X-ray spectra obtained with the FPCS (Vedder and Canizares 1983) and the *EXOSAT* transmission grating (Mewe *et al.* 1986) clearly show emission lines, thus demonstrating the thermal nature of the emission process. We shall consider only spectra produced by plasmas which are in collisional thermal equilibrium, even though in many cases—especially in low signal-to-noise ratio situations—other spectral forms can also produce acceptable fits. At temperatures below $\sim 10^7$ K, most of the energy loss from such a thermal plasma is due to a few emission lines, which the IPC "sees" as merged into a "pseudocontinuum" due to its low spectral resolution. This effect is evident in Figure 1, where we show the single temperature fit for the star 110 Her ([110]; F6 V): the incident, theoretical spectrum is shown in Figure 1*a*, and in Figure 1*b*, plotted for each IPC energy bin are the observed counts (*dots*) and the counts predicted on the basis of the best-fit single temperature model (*histogram*).

Model thermal spectra, describing the emission from an hot, optically thin plasma and suitable for use in the analysis of low-resolution X-ray data, have been calculated by a number of authors (see, e.g., Tucker and Koren 1971; Landini and Monsignori-Fossi 1970, 1984; Kato 1976; Raymond and Smith 1977; Raymond 1985; Gaetz and Salpeter 1983; Mewe 1972; Mewe, Gronenschild, and van den Ord 1985; Shull 1981). In order to test the sensitivity of spectral analyses to the choice of input spectrum, Schmitt *et al.* (1987) compared the results obtained by fitting theoretical spectra calculated by Raymond and Smith (1977) and by Landini and Monsignori-Fossi (1984) to data for a sample of 11 stars and found no significant differences in the derived model parameters. Given the low spectral resolution of the data we are considering, further comparisons of results obtained with different theoretical spectra are not warranted; we will consider only spectra as calculated by Raymond and Smith (1977).

Nevertheless, one must not forget that the calculation of thermal line spectra is a nontrivial task. Raymond (1988) discusses in detail the variety of assumptions and uncertainties underlying the computed X-ray spectra, some of which—such as the assumptions of local isothermality and of Maxwellian electron velocity distribution behavior—may not apply in practice. Clearly, the quality of our data does not allow us to address such issues, and consequently, these considerations are beyond the scope of this paper.

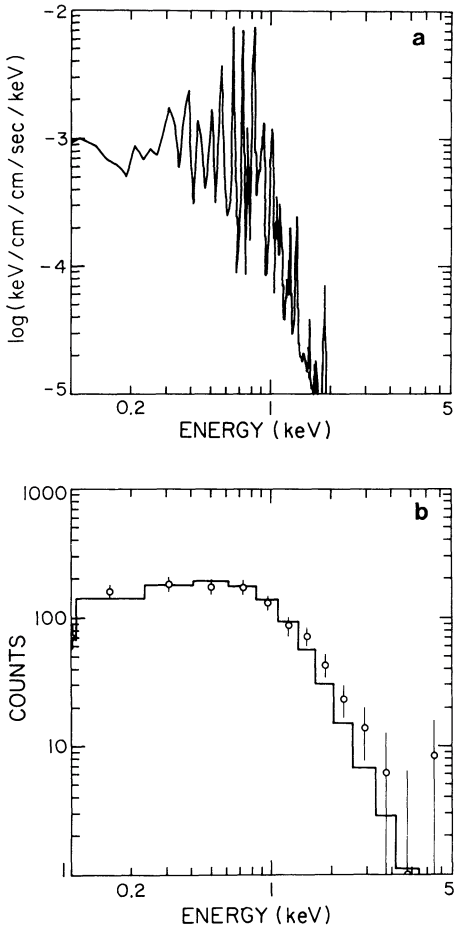

FIG. 1.—Single-temperature, isothermal model fit for the star 110 Her ([110]; F6 V): (*a*) incident theoretical spectrum; (*b*) predicted counts histogram compared with observed counts (*dots*) for each IPC energy bin. The best-fit parameters are $\log T = 6.59$ and $\chi^2_{\rm red} = 1.21$ with 9 degrees of freedom.

b) Model Coronae

The emission from an optically thin plasma can be simply described by an expression of the form

$$F(\lambda) = \frac{1}{4\pi d^2} \int \frac{dT}{T} P(T, \lambda) \frac{n^2 T}{dT/ds} \text{ ergs s}^{-1} \text{ cm}^{-2} \text{ A}^{-1}, \quad (1)$$

where d is the distance to the source, $P(T, \lambda)$ is the plasma emissivity at wavelength λ (Raymond and Smith 1977), n is the plasma density, dT/ds is the temperature gradient, and

$$Q(T) = \frac{n^2 T}{dT/ds}, \quad (2)$$

is the differential emission measure. The key task we face is to deduce the differential emission measure distribution, that is, the amount of material at any given temperature, from observations of $F(\lambda)$. Here we have of course suppressed the additional complications introduced by actually folding the incident spectrum F through the instrument; this is irrelevant for our present purposes since the fundamental mathematical problem is not changed by this additional folding.

Given the low spectral resolution of the IPC and the relatively low signal-to-noise-ratio of our data (at least in some cases), a direct inversion of equation (1) to determine $Q(T)$ is impossible; instead, we have considered five different, but very simple, coronal models for comparison with the observed spectral distribution of the incident X-ray flux:

Model 1.—An *isothermal plasma*, i.e., $Q(T) = \mathrm{EM}_1\ \delta(T - T_1)$, with two adjustable parameters—the temperature T_1, and the differential emission measure at that temperature, which reduces to a single number, namely the emission measure EM.

Model 2.—An *isothermal plasma with intervening absorption*, i.e., with $Q(T) = \mathrm{EM}_1\ \delta(T - T_1)$, and three adjustable parameters—T, EM, and the hydrogen column density N_{H}; since most of the objects in our study are rather nearby, the effects of the absorbing column density N_{H} will turn out to be small, and only in a few cases of somewhat more distant giants, supergiants, and RS CVn systems do we obtain spectral fits with N_{H} significantly different from zero (cf. § IV).

Model 3.—A plasma consisting of *two isothermal components*, with four adjustable parameters—T_1, EM_1, T_2, and EM_2, i.e., $Q(T) = \mathrm{EM}_1\ \delta(T - T_1) + \mathrm{EM}_2\ \delta(T - T_2)$.

Model 4.—A plasma consisting of *two isothermal components at fixed temperatures*, of $\log T_1 = 6.4$ and $\log T_2 = 7.2$, and two adjustable parameters—the corresponding emission measures EM_1 and EM_2), i.e., $Q(T) = \mathrm{EM}_1\ \delta(T - 10^{6.4}) + \mathrm{EM}_2\ \delta(T - 10^{7.2})$.

Model 5.—A plasma with a *continuous emission measure distribution* of the form

$$Q(T) = \mathrm{EM}_{\mathrm{max}}\left(\frac{T}{T_{\mathrm{max}}}\right)^{\alpha}, \tag{3}$$

with three adjustable parameters—the normalization constant $\mathrm{EM}_{\mathrm{max}}$, the maximum temperature T_{max}, and the slope of the emission measure distribution α. This functional form of $Q(T)$, i.e., a power law of the form

$$Q(T) \sim T^{\alpha},$$

turns out to describe the differential emission measure distribution of isolated solar coronal loops very well (cf. Antiochos and Noci 1986); the power-law slope α is related to the power-law coefficient of the radiative cooling function [approximated as $P(T) \sim T^{\beta}$] through

$$\alpha = \frac{3}{4} + \frac{\beta}{2}. \tag{4}$$

Antiochos and Noci (1986) have investigated the expected differential emission measure distributions from single loops and ensembles of loops; for coronal hot loops, they find the differential emission measure distribution dominated by loops with the highest temperature and density, and therefore equation (3) also applies for an ensemble of loops at temperatures in excess of 10^6 K. This property of hot loops justifies our power-law assumption for the differential emission measure distribution, and as an additional benefit, we can interpret the derived parameters T_{max} and α from a physical point of view. If equation (3) applies, it is clear that the choice of the power-law slope α for the differential emission measure distribution is not arbitrary, a fact which both motivated our analysis procedures and justifies our approach.

The reader might well wonder about the number of models we shall be considering. It is important to remember that, although low signal-to-noise ratio stellar spectra are more than adequately represented with the simple coronal models, stellar spectra of high signal-to-noise ratio formally fail attempts at description with such simple models. Indeed, in the case of the sole stellar coronal source which has been spatially resolved (the Sun), direct experience with spectral modeling has revealed a highly complex plasma environment which cannot possibly be characterized by a single temperature and single emission measure value. Thus, we should not be surprised that as spatially unresolved observations gain in signal-to-noise ratio, the amount of detail in the spectra which must be reproduced—reflecting the true complexity of the source plasmas themselves—increases as well. For this reason, it is best to regard the above sequence of coronal models, (1), (3), and (5), simply as a sequence of models incorporating increasing source complexity as the source spectra improve in signal-to-noise ratio.

IV. RESULTS AND DISCUSSION

Our approach to this analysis was to begin with the simplest models, namely the one-temperature coronal models, and then to proceed to greater complexity as the data warrant. Since single and binary stars do not appear to exhibit a markedly different behavior, we decided not to distinguish these two subsamples in the graphical presentation of our results; the information on multiplicity can, however, be found in column (12) of Table 1. Also in Table 1 (col. [13]) are the results of our spectral fitting procedure for each observation; the various possible outcomes indicated by this "fit code" are summarized in Table 6 (cf. § IV*d*).

a) One-Temperature Models

In Table 2, which presents the one-temperature fits for all sample stars which yielded χ^2_{red} (col. [9]) less than 2.5, each observation is identified by IPC sequence number and source number (cols. [1] and [2]), and each star is also cross-referenced to Table 1 with the cross-reference number of column (10). Logarithms of the best-fit temperature and its upward and downward 68% confidence intervals are given in columns (3)–(5). Examination of the derived N_{H} column densities in column (6) (of Table 2) reveals that the fits for most of these stars produced only upper limits on N_{H}, i.e., the X-ray spectra of these stars do not require any absorbing column. In most of the remaining cases, the improvement made by accounting for N_{H} is small, but for eight exceptions (the stars HD 22211 [45], HD 30050 [58], HD 73343 [72], HD 163930 [107], HD 209318 [120], HD 216489 [125], HD 218356 [126], and HD 219113 [127]), a statistically significant improvement in the fit was obtained when finite (as opposed to negligible) values of N_{H} were included in the fits. Emission measures (col. [7]) and the 0.2–4.0 keV flux (col. [8]) are also provided in the table.

i) *X-Ray Temperatures*

In Figure 2 we show—for acceptable one-temperature fits—box plots (cf. Chambers *et al.* 1983) of the resulting X-ray temperature for main-sequence stars with $B-V < 1$, main-sequence stars with $B-V \geq 1$, giants, and RS CVn systems, with this last class further subdivided into "classical" members and those not known to contain giants ("dwarf RS CVn systems" or "BY Dra systems"; cf. Strassmeier *et al.* 1988). Upper and lower ends of the boxes indicate the second and third (inner) quartiles, horizontal lines drawn through the boxes are the medians of the data, and the vertical dashed lines

TABLE 2

ONE-TEMPERATURE FITS

Sequence number (1)	Source number (2)	log T (3)	log T^+ (4)	log T^- (5)	log N_H (6)	$EM\ d_{pc}^2$ 10^{-49}cm^{-3} (7)	f_x 10^{13} erg s^{-1} cm^{-2} (8)	χ^2_{red} (9)	Xref number (10)
350	1	6.42	6.47	6.38	18.5	0.18	4.57	0.96	55
501	3	6.88	6.97	6.65	< 19.0	1.76	41.02	2.48	71
844	9	6.19	6.32	5.94	< 21.4	0.11	2.29	1.23	112
845	2	6.96	7.05	6.90	< 18.4	2.33	53.91	1.82	38
847	4	7.21	7.33	7.11	19.6	2.47	38.11	0.46	65
848	4	6.25	6.27	6.22	< 19.5	3.31	77.40	1.03	67
2225	1	6.59	6.70	6.55	19.4	1.86	41.59	1.23	31
2300	2	7.17	7.25	7.09	< 19.5	3.17	54.83	0.33	36
2302	1	6.98	7.06	6.93	< 18.6	7.93	182.60	1.50	2
2306	1	7.34	7.38	7.31	< 18.3	85.34	1055.00	1.37	46
2310	1	7.22	7.25	7.19	< 19.1	32.03	486.10	0.65	68
2311	1	7.24	7.27	7.21	< 17.9	27.43	401.00	1.34	68
3091	1	7.50	7.78	7.30	< 16.5	3.55	40.28	1.69	17
3113	2	6.40	6.42	6.38	< 19.4	2.61	66.98	1.23	108
3153	6	7.57	7.68	7.47	20.7	3.60	40.13	0.40	120
3191	1	7.12	7.16	7.08	19.0	6.80	130.50	2.10	34
3192	1	7.62	7.71	7.54	< 19.2	43.60	480.30	0.96	35
3195	2	7.41	7.59	7.31	20.8	3.86	45.36	1.29	58
3196	1	7.71	7.93	7.48	20.0	6.46	69.54	0.66	59
3204	2	7.49	7.73	7.32	20.3	3.89	44.24	0.99	72
3208	2	7.29	7.37	7.23	19.0	11.80	157.50	0.66	82
3209	1	7.30	7.61	7.18	< 17.1	1.73	22.55	1.53	83
3211	3	7.70	7.87	7.54	19.2	10.27	110.90	0.78	85
3213	4	7.33	7.37	7.29	< 18.1	36.54	462.00	1.05	88
3219	1	7.14	7.17	7.12	< 17.8	30.33	560.80	2.38	100
3227	1	7.24	7.31	7.19	< 18.9	11.05	161.70	1.80	111
3229	1	7.23	7.46	7.13	20.1	2.34	34.40	0.76	117
3230	2	7.64	7.96	7.38	19.5	8.93	97.82	1.09	122
3231	3	7.43	7.71	7.27	20.2	4.07	47.40	0.72	124
3233	1	7.26	7.30	7.22	19.9	13.33	185.80	1.19	125
3234	1	7.55	7.64	7.49	20.0	28.58	319.90	1.41	127
3235	2	7.20	7.23	7.18	< 17.8	37.82	596.20	2.48	129
3236	1	7.45	7.55	7.39	< 18.3	29.31	338.20	1.10	130
3512	2	6.52	6.61	6.47	< 19.9	1.47	34.48	1.29	52
3530	2	6.67	6.79	6.58	< 20.0	1.10	24.70	0.73	79
3531	2	6.51	6.55	6.47	< 19.6	2.10	49.32	1.20	87
3533	2	7.19	7.25	7.14	19.6	6.16	100.10	0.66	39
3534	3	7.18	7.22	7.14	19.1	6.84	112.60	0.80	34
3535	1	7.17	7.22	7.12	< 18.8	7.07	121.70	0.92	75
3536	1	7.08	7.16	7.01	< 19.1	2.85	59.28	0.85	116
3720	5	7.18	7.30	7.05	< 18.7	0.47	7.88	1.71	63
3811	2	6.48	6.52	6.44	< 19.6	1.36	33.00	1.01	103
4146	4	6.45	6.48	6.43	< 19.5	4.57	113.30	2.11	94
4233	3	7.34	7.66	7.25	20.4	2.44	30.34	0.72	126
4348	3	6.67	6.76	6.60	< 19.5	2.59	58.54	0.57	62
4414	2	6.47	6.50	6.44	< 19.5	0.87	21.19	1.51	9
4448	1	7.17	7.21	7.13	< 18.6	10.22	176.40	1.04	77
4452	4	6.94	6.98	6.91	< 18.5	6.39	148.70	1.92	33
4457	1	6.41	6.44	6.38	< 19.8	0.73	18.4	1.11	86
4496	1	7.34	7.38	7.31	< 18.7	101.70	1259.00	1.25	46
4942	3	7.12	7.24	7.01	< 19.4	0.65	12.49	0.85	57
4948	1	7.26	7.33	7.22	19.5	14.93	208.40	1.27	111
5011	1	7.19	7.22	7.17	19.0	21.57	344.90	2.32	123
5014	3	7.18	7.20	7.16	< 18.3	19.60	327.70	2.48	123
5015	1	7.28	7.32	7.24	< 18.6	27.86	375.00	1.51	123

TABLE 2—*Continued*

Sequence number (1)	Source number (2)	log T (3)	log T^+ (4)	log T^- (5)	log N_H (6)	$EM\ d_{pc}^2$ 10^{-49}cm^{-3} (7)	$f_x\ 10^{13}$ erg s^{-1} cm^{-2} (8)	χ^2_{red} (9)	Xref number (10)
5016	1	7.25	7.29	7.22	< 18.7	18.28	260.00	1.57	123
5184	3	7.28	7.35	7.22	< 18.8	4.14	56.15	1.74	69
5185	4	6.48	6.53	6.44	< 19.8	0.45	10.89	0.86	73
5190	2	6.96	7.02	6.90	< 18.7	2.23	51.61	1.69	80
5191	2	6.51	6.55	6.47	< 19.3	1.98	46.45	1.34	98
5448	4	6.50	6.55	6.46	< 20.1	2.23	52.71	0.58	41
5471	4	7.11	7.21	6.96	< 18.5	1.14	22.28	1.59	60
5485	3	6.48	6.51	6.45	< 19.4	1.11	26.84	1.85	5
5493	4	6.57	6.67	6.50	< 20.3	0.52	11.77	1.09	6
5527	2	6.52	6.59	6.46	< 19.8	0.73	17.06	0.89	11
5538	2	6.43	6.46	6.39	< 19.8	0.67	16.83	0.86	81
5549	2	6.53	6.58	6.49	< 20.6	1.22	28.27	1.69	89
5559	7	6.87	6.90	6.83	< 18.6	3.77	87.99	1.40	91
5576	1	6.47	6.59	6.39	< 21.2	0.10	2.40	0.72	96
5584	4	6.93	7.06	6.79	< 19.1	0.44	10.14	1.21	101
5621	2	6.59	6.64	6.56	< 19.7	0.87	19.54	1.21	110
5640	1	6.97	7.06	6.89	< 18.3	1.00	23.02	1.06	114
5645	4	7.03	7.13	6.94	< 18.2	1.19	26.53	2.28	115
5652	5	6.38	6.41	6.35	< 19.9	0.52	13.37	0.96	119
5991	2	6.53	6.69	6.49	< 19.8	1.07	24.71	1.47	15
5992	2	6.43	6.47	6.39	< 19.9	0.49	12.3	1.66	102
5993	1	6.52	6.60	6.47	< 19.9	0.81	18.95	1.15	113
6080	4	6.47	6.52	6.43	< 19.7	0.43	10.45	1.11	37
6960	6	7.19	7.23	7.16	< 19.1	2.92	47.04	1.71	65
6970	7	7.22	7.25	7.19	19.8	2.54	38.55	0.86	107
7359	1	6.63	6.85	6.54	< 17.2	1.42	31.78	0.92	3
7361	1	6.94	7.05	6.88	< 18.3	3.19	74.22	1.98	3
7362	1	7.43	7.57	7.31	< 18.0	5.89	68.44	0.92	30
7364	1	6.52	6.58	6.47	< 20.6	1.28	29.83	2.36	30
7416	7	6.43	6.48	6.39	< 19.8	0.33	8.21	1.26	22
7471	2	7.27	7.40	7.20	< 18.6	2.56	35.30	1.41	27
7607	4	6.97	7.08	6.89	< 19.3	1.20	27.63	0.62	76
7609	4	6.97	7.01	6.93	< 18.7	1.89	43.78	0.64	97
7610	3	7.03	7.11	6.98	< 19.8	0.66	14.80	0.68	99
7611	6	6.89	6.95	6.82	< 18.9	0.26	5.97	0.97	106
7663	1	6.45	6.50	6.41	< 19.8	1.02	25.24	0.99	103
7710	2	6.58	6.71	6.51	< 18.2	0.62	14.80	0.67	25
7737	4	7.57	7.80	7.41	< 18.0	5.79	64.48	1.07	40
7888	4	6.48	6.52	6.44	< 19.7	1.00	24.33	0.87	105
7913	2	6.65	6.72	6.60	< 18.8	1.28	28.61	1.03	84
7918	6	6.46	6.50	6.43	< 19.6	0.74	18.04	0.35	47
7954	4	6.44	6.48	6.41	< 19.7	0.43	10.58	0.70	74
7958	6	6.53	6.59	6.48	< 20.9	0.42	9.75	1.78	32
8396	7	7.15	7.20	7.11	19.2	2.31	41.17	0.51	128
8397	7	7.01	7.07	6.95	20.6	0.44	9.90	0.96	45
9002	5	6.54	6.59	6.50	< 19.6	0.49	11.29	1.79	50
9005	9	6.58	6.70	6.51	< 18.0	0.29	6.47	0.78	53
9041	1	7.36	7.39	7.33	< 17.7	101.20	1230.00	2.02	43
9042	1	7.40	7.44	7.37	< 17.8	81.28	961.00	2.27	43
9692	3	6.52	6.55	6.49	< 19.5	1.41	33.03	2.32	66
9705	1	6.61	6.73	6.53	< 18.1	0.57	12.79	0.62	90
9711	1	6.55	6.64	6.49	< 20.1	0.48	10.93	1.17	121
10100	2	6.57	6.64	6.50	< 20.4	0.54	12.19	0.40	70
10538	8	7.07	7.16	6.99	20.0	1.28	27.32	0.56	56

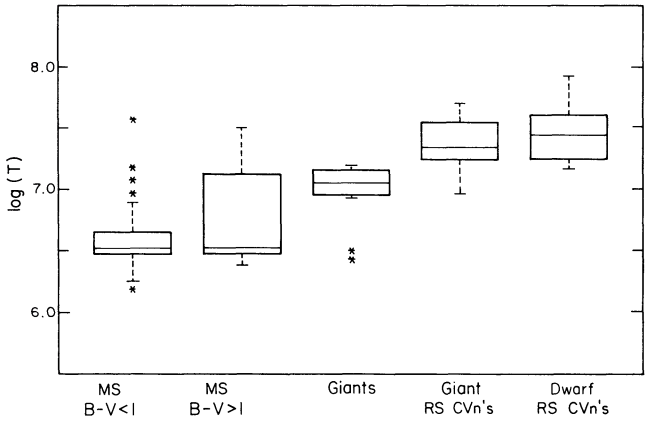

FIG. 2.—Box plots of coronal temperatures for successful one-temperature fits (with floating N_H) to data from five classes of stars, from left to right: main-sequence stars with $B-V \leq 1$, main-sequence stars with $B-V > 1$, giants, and RS CVn systems, separated into those containing giants and those containing dwarfs (viz. BY Dra systems). Upper and lower ends of the boxes indicate the second and third quartiles, horizontal lines drawn through the boxes are the medians of the data, vertical dashed lines encompass all points within the so-called inner fences of the data (see § IV of text), and "outliers" are explicitly plotted with asterisks.

encompass all points within the so-called inner fences (points 1.5 times the inner-quartile spread, above and below the boxes; see, e.g., Tukey 1977); "outliers"—points beyond the inner fences—are explicitly plotted with asterisks. The one-temperature fits assumed a "floating" value of N_H, but if N_H was found not to be significantly different from zero, it was not included in the number of degrees of freedom.

As is obvious from Figure 2, main-sequence K and M stars with $B-V \geq 1$ exhibit a large spread in coronal temperature. For these stars, however, all successful one-temperature fits obtain for low signal-to-noise data (as will be demonstrated in Fig. 4); high signal-to-noise spectra for these types of stars always show evidence for a multi- and high-temperature plasma. Main-sequence stars with $0.2 < B-V < 1$ (*not* plotted separately in Fig. 2) are characterized by rather low coronal temperatures, much like the quiet Sun. Only six of 32 such stars have coronal temperatures outside the range from 1.7×10^6 K to 4.7×10^6 K (HD 17138 [40], HD 37495 [63], HD 28867 [56], HD 196524 [114], HD 11443 [38], and HD 187642 [112], here listed in order of decreasing temperature).

Since eight of our main sequence stars with $B-V > 1$ ([1], [8], [10], [14], [16], [17], [24], [25]) showed indications of broad-band flux variability (greater than 4 σ confidence in the "secular test" of the standard IPC REV-1 Section 8 printout; cf. page 199 of Harnden *et al.* 1984), we examined these data for connections between this variability and possible changes in spectral hardness. Although the median temperatures for variable main-sequence stars are somewhat higher than those of the nonvariable stars, a Kolmogorov-Smirnov test showed no significant effect.

In contrast to the cooler main-sequence stars, giants seem to have fairly hot coronae, with temperatures in excess of 10^7 K, more reminiscent of the flaring Sun. Two of the 16 giants represented in Figure 2 consitutute exceptions to this general trend; shown as outliers in the figure, they are both low–X-ray luminosity, apparently single, F-type giants (α Crv [81] and α Cha [70]). (Note that giants later than K0 do not seem to emit X-rays at currently detectable levels (Vaiana *et al.* 1981; Ayres *et al.* 1981; Haisch and Simon 1982; Haisch 1987; Gondoin, Mangenay, and Praderie 1987; Maggio *et al.* 1990): no giants with $B-V$ greater than ~ 1 are present in our sample.) No large-amplitude variability is present in any individual observations of giants, thus excluding obvious flaring activity as the cause of the high temperatures, although we cannot exclude the possibility of a large number of small flares being responsible for the observed hot plasma and remaining undetected.

The fact that high coronal temperatures appear to be a characteristic of the quiescent X-ray emission from giants has interesting implications for models of the quiescent coronae of such low-gravity stars. These high temperature components do not appear to be accompanied by corresponding low-temperature components, as is the case for main-sequence stars with $B-V > 1$, but rather, the coronae of giant stars are found to be quite isothermal (at least in our bandpass), with extremely large temperatures. The transition from chromospheric and transition region temperatures to coronal temperatures must thus be very abrupt, with very little emission measure present at intermediate ($\approx 10^6$ K) temperatures. Interestingly enough, the X-ray temperatures for giants in binary systems do still show the same characteristics as single giants, i.e., temperatures in excess of 10^7 K, and no accompanying low-temperature component. We therefore conjecture that in those systems the X-ray emission is actually dominated by the emission from the giant component. As a final caveat, we emphasize that the above considerations apply only to giants with X-ray luminosities larger than the median X-ray luminosity; for lower luminosity giants, we lack detailed spectral information.

Finally, the RS CVn stars as a group show extremely high X-ray temperatures (in the range between $7.2 < \log T < 7.7$), significantly hotter than giant stars. We note that some of these objects show evidence for a multitemperature plasma and are therefore included in Figure 7 (rather than in Fig. 2). As indicated in Figure 2 (and also in Fig. 10 below), we have investigated possible differences between RS CVn systems that contain giants ("classical" members of this class) and those sometimes termed "BY Dra systems" (Strassmeier *et al.* 1988) which are *not* known to contain a giant star. However, because our sample contains only six of the latter systems (cf. Category "dR" in Table 1), we are unable to demonstrate any significant differences between these two subcategories.

ii) *X-Ray Temperature versus Luminosity*

From the normalization constant of a one-temperature fit, an emission measure and hence an X-ray luminosity can be computed; Figure 3 shows the resulting X-ray luminosities as a function of X-ray temperature. The X-ray luminosity L_x (0.2–4 keV) and coronal temperature T appear to be correlated, with $L_x \sim T^{2.5}$, similar to results previously reported by Vaiana (1983). We do need to caution, however, that it is unclear to what extent this correlation results from a physical cause, rather than from observational selection. Selection effects certainly are present in Figure 3: whereas high-luminosity objects with low coronal temperature were detectable in our survey (although none was found), low-luminosity objects with high temperatures could well have been missed. In fact, such objects do exist (i.e., nearby M dwarfs), but these objects tend to show a more complicated temperature structure, which is not well described by the single-temperature models. Because the IPC was not sensitive enough to collect more than 200 counts for low-luminosity (i.e., below $\log L_x \sim 29$) giants which might also populate this part of Figure 3, we do not presently know

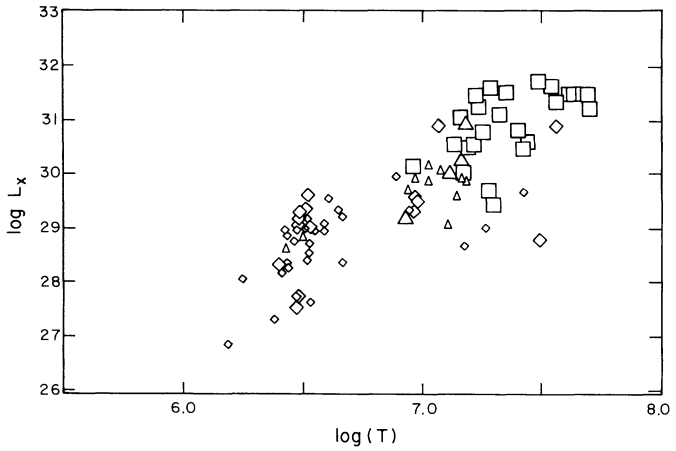

FIG. 3.—X-ray luminosity L_X vs. T for successful one-temperature fits. Diamonds denote main-sequence stars, triangles denote giants, and open squares denote RS CVn systems; small symbols are used for single stars, and large symbols, for binary systems.

the coronal temperatures of these objects (cf. Maggio *et al.* 1990), which presumably could have temperature similar to those of main sequence stars of similar X-ray luminosity.

Finally, we note the existence of an obvious gap in the X-ray temperature distribution, between $6.7 < \log T < 6.9$, in which we derived no X-ray temperatures. From our spectral simulations (cf. Appendix C), we are confident that if isothermal coronae with temperatures in this range existed, we could have determined their temperatures with the IPC. We therefore believe that this gap arises (at least in part) from intrinsic properties of the differential emission measure distribution of coronal X-ray sources and not solely from the spectral response characteristics of the IPC.

b) Two-Temperature Models

Because the amount of information that can be extracted from an X-ray spectrum must depend on the number of photons collected, it is sensible to ask to what extent the adequacy of a one- or two-temperature description is simply a matter of signal-to-noise ratio. To answer this question, we plot in Figure 4 (which shows multiple points for objects observed more than once) the number of IPC counts in the successful one- and two-temperature spectral fits as a function

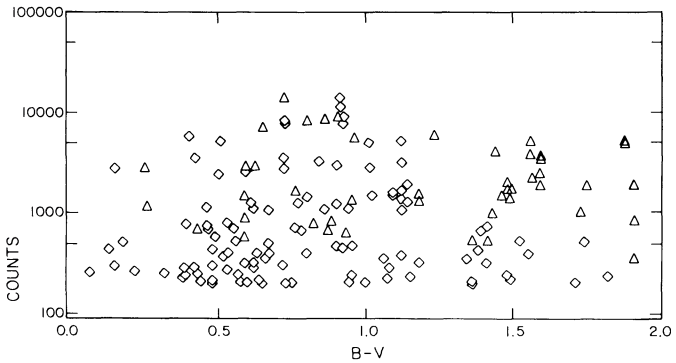

FIG. 4.—Number of counts in IPC spectrum vs. $B-V$ color for all sample stars; diamonds denote successful one-temperature fits, triangles, successful two-temperature fits. Note that multiple points are shown for objects observed more than once.

of $B-V$ color. Three effects are immediately apparent from Figure 4.

1. IPC spectra containing less than ~ 500 counts can always be adequately described with a one-temperature model (the sole exception being a ~ 400 count observation of UV Ceti; [1]—cf. Table 1).

2. M stars ($B-V > 1.2$) and more than ~ 800 IPC counts always require a two-temperature description (a result found for all 22 observations of 13 such stars).

3. Some high signal-to-noise ratio observations of stars with $B-V < 1$ require only a single-temperature description, while others require a two-temperature models.

This last statement has implications for the issue of variability in RS CVn systems. Twenty-four observations of 14 surveyed binaries are divided approximately equally between those requiring only a single component and those requiring two temperatures; but all three of the RS CVn systems observed more than once (UX Ari [43], V711 Tau [46], and AR Lac [123]) fell into *both* of these categories, a fact we interpret as an indication of spectral variability. We note also that the 0.2–4 keV fluxes of both V711 Tau and AR Lac varied between observations: by 19% (at 12 σ confidence) for V711 Tau (cf. Table 5, sequences 2306 and 4496), and by 42% (16 σ) for AR Lac (cf. Table 5, sequences 5015 and 5016).

To be more quantitative, we present in Table 3 the results of acceptable two-temperature fits for those sample stars which could not be adequately described with the one-temperature model. Columns (1)–(5) and (7) and (8) of Table 3 follow the first seven columns of Table 2 (presenting parameters for the low-temperature component of the model), while columns (8)–(12) provide analogous information for the high-temperature component. The last two columns of the two tables also correspond.

In Figure 5 we compare the one- and two-temperature fits for the star AU Mic ([21]; M0e V); the improvement in data description provided by the two-temperature model is evident (see figure legend).

As for the single-temperature case, we set our two-temperature fit acceptance criterion as $\chi^2_{\rm red} < 2.5$; note that systematic errors are not included in the χ^2 computation (cf. Appendix B). Because other acceptance criteria may lead to different samples, we have plotted in Figure 6 (which shows multiple points for objects observed more than once) the distribution of $\chi^2_{\rm red}$ as a function of the number of counts in the X-ray spectrum. Inspection of the figure reveals that for IPC spectra with fewer than ~ 500 counts, the values of $\chi^2_{\rm red}$ tend to be small; for spectra containing more than ~ 1000 counts, the $\chi^2_{\rm red}$ values for one-temperature fits are higher than those for two-temperature fits or for the continuous emission measure distribution fits (to be discussed below). A significant number of objects, however, have acceptable one-temperature fits "despite" their large signal-to-noise ratio, and Figure 6 shows that this number does not depend sensitively on the acceptance criterion chosen. We note, however, that some objects cannot be fitted with any spectral model (cf. § IV*d*).

As a consequence, we conclude that little can be said about coronal temperature stratification in IPC sources containing less than ~ 500 counts; on the other hand, the adequacy of one-temperature fits in a number of good signal-to-noise ratio spectra of stars with $B-V < 1$ (mainly giants and RS CVn systems) may actually reflect a different emission measure distribution with respect to stars with $B-V > 1$ (largely main-sequence dMe stars).

TABLE 3

TWO-TEMPERATURE FITS

Sequence number (1)	Source number (2)	log T_1 (3)	log T_1^+ (4)	log T_1^- (5)	$EM_1\ d_{pc}^2$ 10^{-49}cm^{-3} (6)	$f_1\ 10^{13}$ erg s^{-1} cm^{-2} (7)	log T_2 (8)	log T_2^+ (9)	log T_2^- (10)	$EM_2\ d_{pc}^2$ 10^{-49}cm^{-3} (11)	$f_2\ 10^{13}$ erg s^{-1} cm^{-2} (12)	χ^2_{red} (13)	Xref (14)
838	1	6.45	6.46	6.38	2.54	63.00	7.45	7.70	7.23	7.21	83.20	0.610	7
849	1	6.40	6.49	6.24	6.50	166.00	6.90	7.01	6.88	43.80	1020.00	2.280	61
865	3	6.50	6.56	6.39	1.08	25.60	7.35	7.71	7.16	2.07	25.40	0.530	49
905	7	6.35	6.40	6.18	0.50	12.70	7.35	7.79	7.17	1.52	18.70	1.690	1
906	3	5.80	6.33	-5.00	1.30	2.06	7.20	7.55	7.06	1.71	26.90	0.260	1
907	1	6.40	6.43	6.27	1.52	38.70	7.20	7.25	7.14	6.13	96.60	1.510	8
908	3	6.50	6.54	6.47	1.55	36.80	7.40	7.62	7.30	5.09	60.20	1.860	8
917	4	6.45	6.49	6.32	0.62	15.30	7.30	7.42	7.14	1.97	25.80	2.400	13
927	1	6.45	6.47	6.40	2.22	55.10	7.20	7.23	7.15	6.76	107.00	1.080	18
933	1	6.40	6.44	6.37	2.19	55.80	7.25	7.34	7.18	4.42	62.60	0.850	24
2308	1	6.45	6.56	6.19	2.02	50.00	7.10	7.20	7.03	5.73	115.00	1.390	7
2314	1	6.40	6.46	6.36	4.66	119.00	7.30	7.47	7.27	37.30	488.00	2.440	21
3048	6	6.40	6.41	6.31	1.37	35.00	7.20	7.24	7.06	2.34	36.90	1.660	8
3106	1	5.95	6.36	5.29	1.77	14.40	6.95	7.12	6.87	4.02	93.50	2.240	44
3243	3	6.40	6.44	6.34	1.75	44.70	7.20	7.24	7.14	6.02	94.80	1.610	14
3365	4	6.50	6.52	6.44	1.03	24.50	7.25	7.27	7.19	5.50	77.90	1.280	29
3366	1	6.40	6.45	6.39	3.61	92.10	7.20	7.30	7.19	13.90	220.00	2.000	95
4347	2	5.80	6.36	-5.00	2.46	3.91	7.00	7.10	6.90	2.45	56.20	0.150	64
5012	3	6.55	6.65	6.52	2.33	53.10	7.25	7.31	7.24	22.10	313.00	1.980	123
5013	3	6.60	6.63	6.55	4.02	89.80	7.30	7.34	7.25	18.30	240.00	2.180	123
5189	1	6.40	6.45	6.34	5.90	150.00	7.10	7.15	7.04	8.62	174.00	1.250	78
5484	2	6.45	6.48	6.33	1.64	40.50	7.35	7.77	7.10	2.88	35.40	1.120	4
5605	2	6.30	6.47	5.45	0.26	6.50	7.05	7.24	6.95	1.31	28.70	1.180	104
5990	1	6.45	6.51	6.38	1.19	29.40	7.20	7.74	7.06	1.98	31.10	1.330	12
6953	4	6.40	6.45	6.35	0.78	19.90	7.25	7.42	7.16	2.64	37.40	1.760	1
6964	6	6.45	6.51	6.36	1.24	30.70	7.05	7.29	6.91	0.87	19.10	1.770	71
6969	5	6.45	6.47	6.41	0.66	16.30	7.45	7.82	7.27	1.39	16.00	1.770	13
6972	1	6.45	6.46	6.39	3.27	81.10	7.35	7.40	7.27	14.20	174.00	1.070	24
6973	2	6.45	6.46	6.40	2.80	69.50	7.35	7.45	7.30	8.42	103.00	1.140	24
7360	1	6.50	6.57	6.47	1.71	40.60	8.20	-8.25	7.58	3.92	37.40	1.400	3
7363	2	6.10	6.40	5.28	0.20	3.57	7.15	7.28	7.07	1.76	31.60	0.890	30
7380	2	6.30	6.39	5.97	2.21	54.60	7.15	7.24	7.10	10.60	191.00	0.920	23
7381	2	6.45	6.49	6.41	3.47	86.00	7.30	7.43	7.22	9.01	118.00	1.020	23
7382	1	6.35	6.40	6.15	1.90	48.50	7.30	7.44	7.22	8.12	106.00	0.630	23
7605	6	6.45	6.49	6.36	0.60	14.80	7.25	7.36	7.08	1.08	15.30	0.810	118
7606	2	6.35	6.44	5.97	0.34	8.77	7.15	7.42	7.01	0.93	16.60	1.930	48
7689	3	6.50	6.53	6.45	1.85	43.80	7.30	7.34	7.25	6.97	91.20	2.130	14
7748	3	6.35	6.41	6.11	0.78	20.00	7.25	7.28	7.24	15.20	215.00	1.950	26
7749	5	6.30	6.49	5.97	0.26	6.52	7.00	7.14	6.96	1.46	33.50	2.180	28
9004	6	6.40	6.50	6.11	0.46	11.70	7.10	7.20	7.05	2.00	40.40	1.610	51
9005	5	6.20	6.45	5.53	0.13	2.91	6.95	7.07	6.88	0.85	19.70	1.280	52
9006	7	5.70	6.29	-5.00	0.39	0.14	7.05	7.12	6.95	0.45	9.85	1.250	54
9065	3	6.25	6.40	5.72	0.52	12.20	7.05	7.17	6.95	1.50	32.90	1.140	42
9967	1	6.50	6.55	6.43	3.57	84.70	7.45	7.51	7.39	60.40	697.00	2.110	43
10311	2	6.35	6.40	6.02	0.78	20.00	7.20	7.48	7.07	1.84	29.00	0.970	19
10312	2	6.45	6.50	6.43	1.03	25.50	7.30	7.71	7.22	1.93	25.30	0.950	20
10418	1	6.45	6.46	6.39	4.36	108.00	7.30	7.52	7.13	5.83	76.20	1.200	94
10640	2	6.45	6.48	6.37	1.73	42.80	7.20	7.23	7.12	5.02	79.10	1.200	8

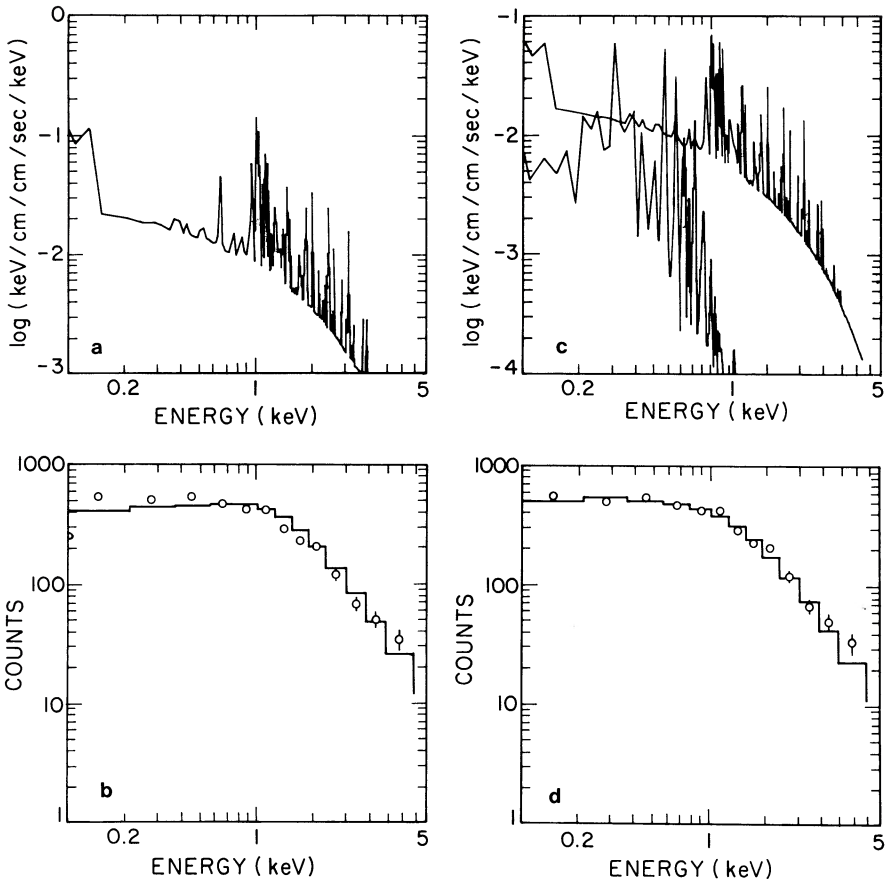

FIG. 5.—Model fits to the X-ray spectrum of the star AU Mic ([21]; spectral type M0e V) for the one-temperature model, in panels (*a*) and (*b*), and the two-temperature model, in panels (*c*) and (*d*). For each model, the incident theoretical spectra are shown in the upper panels, and the observed (*dots*) and predicted (*solid histograms*) counts are compared in the lower panels for each IPC energy bin. In panel (*b*), the single-component model is seen to underpredict the low-energy counts, while in panel (*d*) the two-temperature model is more successful at predicting the entire spectrum. The inclusion of a low-temperature component, shown separately from the high-temperature component in panel (*c*), accounts for the improved fit. Best-fit parameters: for panel (*b*), log $T = 7.20$, emission measure (EM) = 42.4 (same units as Tables 2 and 3), and $\chi^2_{red} = 8.7$ for 11 degrees of freedom; for panel (*d*), log $T_1 = 6.40$, log $T_2 = 7.30$, $EM_1 = 4.6$, $EM_2 = 37.3$, and $\chi^2_{red} = 2.44$ for 9 degrees of freedom.

i) *X-Ray Temperatures*

We now turn to a summary of our two-temperature spectral fitting results. From Figures 4 and 6, it is clear that such models fit well to X-ray spectra with relatively high signal-to-noise ratios. In Figure 7 we show a box plot of the two-temperature components. Note that we have plotted only those cases for which the one-temperature description was found to be unacceptable. A two-temperature description is required for some main-sequence stars, namely those redder than $B-V \sim 0.5$; but despite the availability of a few spectra with good signal-to-noise ratio, single giants hardly ever require two temperature components (the sole exception being θ^1 Tau [52]).

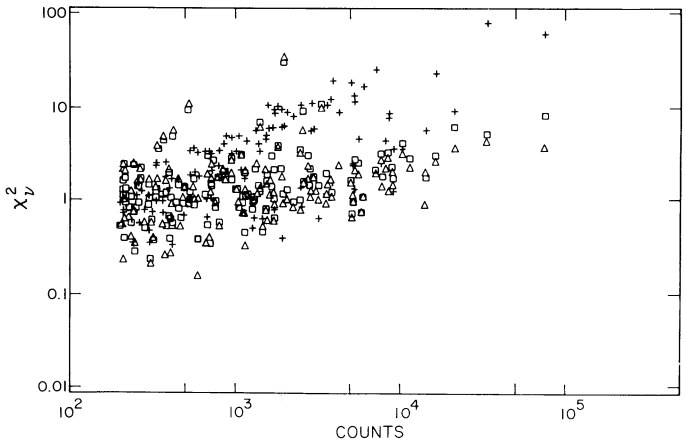

FIG. 6.—χ^2_{red} vs. number of counts in the IPC spectrum for all our sample stars; crosses denote one-temperature fits, triangles, two-temperature fits, and open squares, continuous emission measure distribution fits. Note that multiple points are shown for objects observed more than once.

The temperature components cluster around values of log $T \sim 7.2$ and log $T \sim 6.4$, with some dispersion; in most cases, the errors in the temperature determination (cf. Appendix A) are so large that the deviations from these "standard" values are not significant. In many late-type stars, the appearance of a high-temperature component is linked to the presence of a low-temperature component, with the actual values of these temperatures showing little variation for our IPC measurements.

The fact that two temperature components are often required for spectral fits to IPC data has been noted previously by a number of authors (Vaiana 1983; Schmitt 1984; Majer *et al.* 1986). In particular, Schmitt (1984) and Majer *et al.* (1986) pointed out that two such temperature components—after

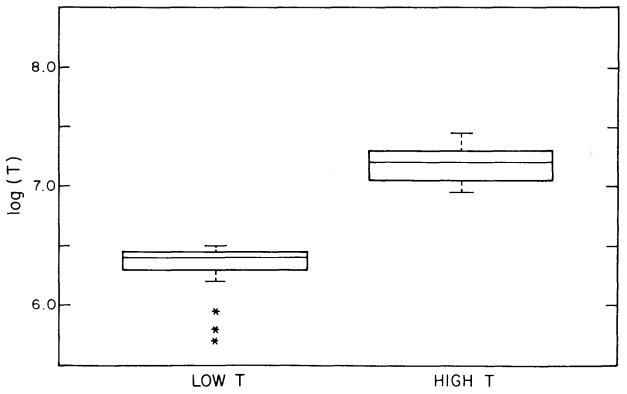

FIG. 7.—Box plots of coronal temperatures for stars in our sample requiring two-temperature components; see Fig. 2 for an explanation of symbols.

conversion to equivalent energy—correspond to regions of the IPC's peak sensitivity, reflecting the instrument's response to a complex flux distribution. Hence such temperatures are not to be interpreted too literally (cf. Appendix C), but rather as "effective temperatures" in the sense discussed by Underwood and McKenzie (1977).

The number of RS CVn systems requiring a two-temperature description is rather small; however, the IPC cannot discriminate plasma temperatures above log $T \sim 7.6$ particularly well. Note in particular that the only RS CVn system in Table 3 with both temperature components below 10^7 K is Capella, which appears to be quite exceptional when compared to other RS CVn systems.

ii) *Emission Measure versus Temperature*

In Figure 8 we plot the ratio of the emission measures derived for the high- and low-temperature components for single stars, binaries, and RS CVn systems, but in order to make a better comparison of the emission measures contained in the two components, we have performed these spectral fits by keeping the two temperatures fixed at log $T = 6.4$ and log $T = 7.2$ (coronal model [4] of § III*b*). This procedure, the results of which are reported in Table 4, is justified by noting that the normalization constants, which are highly correlated with the derived temperature values, are treated as "uninteresting" parameters (from a statistical point of view) in the two-temperature fits. By fixing the two temperatures, we can obtain results for cases in which a single temperature description with a "floating" temperature might also have sufficed. In the table, we again identify observations through IPC sequence and source number (cols. [1] and [2]) and provide a cross-reference number in the last column. The derived low- and high-temperature emission measures are given in columns (3) and (5), columns (4) and (6) contain the 0.2–4.0 keV fluxes in the two components, and column (7) gives the derived χ^2_{red} of the fit.

No trend with color is apparent when all stars of Figure 8 are considered, but trends within classes (distinguished with different plotting symbols) are apparent: giant stars (with two exceptions: α Crv [81] and α Cha [70]) are characterized by rather large ratios of the high-temperature component emission measure to the low-temperature component emission measure. This result is, of course, consistent with our earlier finding that giants can be fitted with an isothermal model at high temperature with no need for lower temperature material. The same remarks also apply to the RS CVn systems.

c) Continuous Emission Measure Distributions

In Table 5 we present the fit results for the continuous emission measure distribution model of equation (3). As before, we identify the observations with IPC sequence and source number in the first two columns and provide a cross-reference number in the last. Columns (3)–(5) give log T_{max} and its 68% confidence interval, and columns (6)–(8) give α and its confidence interval. The 0.2–4.0 keV flux and χ^2_{red} appear in columns (9) and (10).

Our spectral results for continuous emission measure distribution fits are summarized graphically in Figure 9: Figure 9*a* contains a box plot of the fitted values of T_{max}, and Figure 9*b* provides the information on the fitted power-law slopes α. Note that here we have displayed T_{max} and α results even for those stars which had acceptable one-temperature descriptions, since the single-temperature model may be thought of as an emission measure distribution with infinite slope α. Figures 9*a* and 10 (see below) show a much larger spread of temperatures than the corresponding Figures 2 and 3; temperatures as high as log $T = 8.2$ are allowed by the data within the framework of a continuous emission measure distribution model, although in all such cases the errors are quite large and

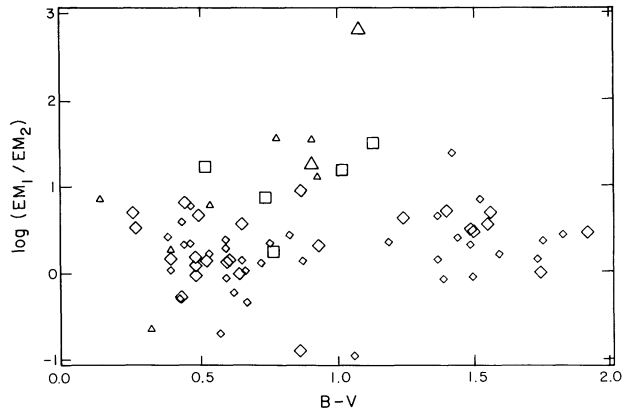

FIG. 8.—Logarithmic ratio of high- to low-temperature emission measures for sample stars which can be fitted with the two-component model with fixed temperatures at log $T = 6.4$ and log $T = 7.2$; symbols as in Fig. 3.

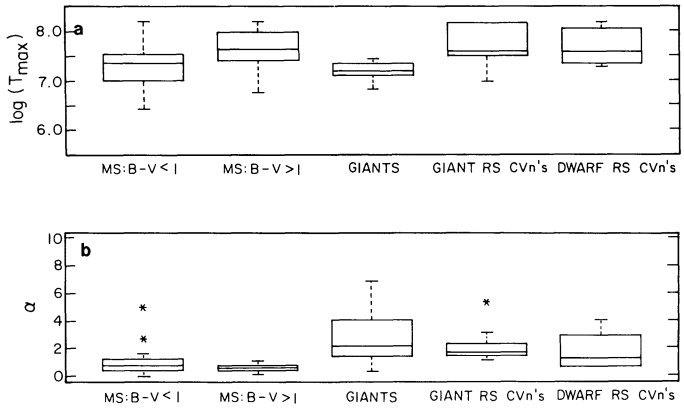

FIG. 9.—Box plots of T_{max} (*a*) and α (*b*) for stars with successful continuous emission measure distribution fits (see legend of Fig. 2 for box plot description).

TABLE 4

EMISSION MEASURE FITS

Sequence number (1)	Source number (2)	$EM_1\ d_{pc}^2$ 10^{-49}cm^{-3} (3)	$f_1\ 10^{13}$ erg s^{-1} cm^{-2} (4)	$EM_2\ d_{pc}^2$ 10^{-49} cm^{-3} (5)	$f_2\ 10^{13}$ erg s^{-1} cm^{-2} (6)	χ^2_{red} (7)	Xref number (8)
350	1	0.14	3.57	0.07	1.16	1.320	55
501	3	0.74	18.70	1.90	30.00	1.650	71
838	1	1.80	45.80	5.64	88.80	0.830	7
845	2	0.56	14.20	2.67	42.10	1.450	38
865	3	0.70	17.90	1.98	31.20	0.690	49
905	7	0.67	17.00	0.95	15.00	2.360	1
906	3	0.87	22.10	1.21	19.10	1.060	1
907	1	1.52	38.70	6.13	96.60	1.510	8
917	4	0.45	11.40	1.77	27.80	2.410	13
927	1	1.69	43.00	7.31	115.00	1.440	18
933	1	2.15	54.70	3.97	62.50	0.930	24
2225	1	0.76	19.40	1.72	27.20	1.750	31
2302	1	1.82	46.30	9.48	149.00	0.950	2
2311	1	0.74	18.80	23.70	374.00	1.360	68
3048	6	1.37	35.00	2.34	36.90	1.660	8
3091	1	0.41	10.50	1.53	24.10	1.580	17
3113	2	2.45	62.30	0.32	5.06	1.490	108
3209	1	0.15	3.78	1.12	17.70	1.960	83
3219	1	1.90	48.40	32.70	515.00	2.170	100
3227	1	0.19	4.76	9.75	154.00	2.470	111
3235	2	2.16	54.90	34.30	541.00	0.920	129
3243	3	1.75	44.70	6.02	94.80	1.610	14
3365	4	0.59	15.00	5.38	84.90	1.590	29
3366	1	3.61	92.10	13.90	220.00	2.000	95
3512	2	0.62	15.90	1.29	20.30	1.040	52
3530	2	0.62	15.70	0.84	13.20	1.640	79
3531	2	1.21	30.80	1.09	17.20	1.670	87
3535	1	0.20	4.98	7.44	117.00	1.220	75
3536	1	0.10	2.48	3.66	57.70	1.460	116
3720	5	0.07	1.69	0.40	6.28	1.250	63
3811	2	0.79	20.20	0.78	12.30	0.600	103
4146	4	3.31	84.40	1.52	23.90	2.470	94
4347	2	1.82	46.30	2.48	39.00	0.710	64
4348	3	1.25	31.90	2.17	34.20	2.000	62
4414	2	0.54	13.70	0.46	7.26	1.100	9
4448	1	0.54	13.70	10.30	162.00	1.030	77
4457	1	0.63	16.10	0.13	2.03	1.640	86
4942	3	0.00	0.03	0.81	12.70	1.360	57
5016	1	0.22	5.55	15.70	248.00	2.410	123
5185	4	0.26	6.63	0.27	4.22	0.860	73
5191	2	0.97	24.80	1.39	21.90	0.880	98
5448	4	1.03	26.10	1.29	20.40	1.570	41
5471	4	0.16	4.03	1.20	18.90	1.800	60
5484	2	1.21	30.70	2.58	40.70	1.140	4
5485	3	0.64	16.20	0.67	10.50	1.060	5
5493	4	0.24	6.04	0.41	6.50	2.180	6
5527	2	0.36	9.18	0.53	8.36	0.660	11
5538	2	0.55	14.00	0.13	2.08	1.370	81
5549	2	0.58	14.70	0.90	14.30	1.110	89
5576	1	0.05	1.31	0.07	1.17	0.690	96
5605	2	0.49	12.60	1.65	26.00	1.400	104
5621	2	0.35	8.87	0.76	12.00	1.550	110
5640	1	0.19	4.85	1.25	19.70	0.870	114
5645	4	0.22	5.55	1.40	22.00	2.330	115
5652	5	0.51	13.10	0.06	0.92	1.580	119
5990	1	0.88	22.30	2.30	36.30	1.620	12
5991	2	0.43	11.10	0.93	14.70	0.960	15
5993	1	0.40	10.10	0.57	9.06	1.470	113
6080	4	0.24	6.25	0.27	4.26	0.900	37
6953	4	0.77	19.60	2.34	36.90	1.800	1
6969	5	0.48	12.20	1.12	17.70	1.990	13
6972	1	2.28	58.00	11.60	183.00	2.290	24
6973	2	2.04	52.10	7.05	111.00	2.160	24
7359	1	0.56	14.40	1.41	22.20	0.650	3

TABLE 4—*Continued*

Sequence number (1)	Source number (2)	$EM_1\ d_{pc}^2$ 10^{-49}cm^{-3} (3)	$f_1\ 10^{13}$ erg s^{-1} cm^{-2} (4)	$EM_2\ d_{pc}^2$ 10^{-49} cm^{-3} (5)	$f_2\ 10^{13}$ erg s^{-1} cm^{-2} (6)	χ^2_{red} (7)	Xref number (8)
7360	1	0.86	21.90	2.89	45.50	2.060	3
7361	1	0.83	21.00	3.80	59.90	1.230	3
7362	1	0.15	3.79	3.67	57.80	2.190	30
7363	2	0.57	14.50	1.73	27.30	1.090	30
7364	1	0.55	13.90	1.13	17.80	1.330	30
7380	2	3.92	99.90	10.80	170.00	1.100	23
7381	2	2.53	64.50	8.25	130.00	1.190	23
7382	1	2.46	62.70	6.05	95.30	1.730	23
7416	7	0.21	5.39	0.20	3.11	1.100	22
7471	2	0.25	6.29	1.75	27.60	1.190	27
7605	6	0.45	11.40	1.12	17.60	0.970	118
7606	2	0.48	12.20	0.95	14.90	1.960	48
7607	4	0.12	3.17	1.71	26.90	1.100	76
7663	1	0.75	19.10	0.34	5.28	1.620	103
7710	2	0.23	5.74	0.64	10.00	0.390	25
7888	4	0.69	17.50	0.37	5.88	1.320	105
7918	6	0.50	12.70	0.30	4.73	0.460	47
7954	4	0.31	8.03	0.15	2.33	0.750	74
7958	6	0.25	6.26	0.27	4.19	2.160	32
9002	5	0.21	5.28	0.42	6.68	1.010	50
9004	6	0.50	12.80	2.55	40.20	2.390	51
9005	9	0.12	2.94	0.27	4.28	0.640	53
9006	7	0.14	3.54	0.54	8.57	1.730	54
9065	3	1.12	28.50	1.61	25.30	1.350	42
9692	3	0.66	16.80	1.00	15.70	2.010	66
9705	1	0.21	5.34	0.55	8.70	0.720	90
9711	1	0.20	4.99	0.42	6.63	1.530	121
10100	2	0.21	5.35	0.41	6.40	2.420	70
10311	2	1.07	27.30	1.59	25.10	1.290	19
10312	2	0.75	19.20	1.84	29.00	1.260	20
10418	1	3.24	82.40	5.84	92.00	1.260	94
10640	2	1.30	33.10	5.46	86.10	1.580	8

we therefore do not claim to have direct observational evidence for such hot gas. (Note also that temperatures of $\log T = 8.2$ were the largest ones considered in our fits, and that at such large temperatures most of the emission falls outside the IPC bandpass, making it virtually impossible to constrain the properties of the emitting plasma.)

Figure 9 demonstrates that the high-temperature components found in a two-temperature fit do not necessarily reflect the largest possible temperature present in a given stellar corona. Obviously, the temperatures obtained by applying equation (3) are model-dependent, but they do indicate that the range of coronal temperatures encountered in stars may not be as narrow as a one- or two-temperature analysis seems to suggest. Main-sequence stars appear to cluster at values of $\alpha \sim 0.8$, with a very small dispersion for stars with $B-V > 1$. Those with $B-V < 1$ tend to have a larger dispersion in α, and their temperatures are on average lower than the temperatures of K and M dwarfs. Rather large values of α (viz., larger than 1) are found for low-gravity objects, i.e., giants and RS CVn systems, which are certainly *nonsolar*. That this conclusion does not depend on any instrumental effects is demonstrated in a series of simulations reported in Appendix C. Our fits to simulated, low signal-to-noise ratio IPC spectra with slopes α in excess of 1 inferred even larger values for α, demonstrating a positive bias in the fitted power-law slopes. However, that bias is significant only for large values of α, and therefore the median values of the α distributions for giants and RS CVn systems are definitely larger than 1. Large values of α are, of course, a reflection of the fact that most of the emission is concentrated at the maximum temperature, consistent with our earlier finding that the single-temperature description was acceptable for these objects.

We emphasize that these large values of α are not attributable to absorption of a possible lower temperature component: the single-temperature fits to the three giants in Figure 9*b* with the largest values of α have already shown that no intervening absorption is required. While main-sequence stars have IPC spectra consistent with predictions from the simplest coronal models (Antiochos and Noci 1986) and with differential emission measure distributions of slopes similar to those measured for the Sun, it appears that the X-ray spectra of giants and RS CVn systems are markedly different. The groups of RS CVn systems is clearly singled out, yielding extremely high temperatures and definitely "nonsolar" values of α. The only exception to this appears to be Capella [61], which by comparison shows evidence only for rather low temperatures.

In Figure 10 we display the results of Figure 9 in more detail by plotting α as a function of T_{max}, denoting early ($B-V < 1$) and late ($B-V > 1$) main-sequence stars with the symbols "e" and "l," respectively, and giants and RS CVn systems, with

TABLE 5

CONTINUOUS EMISSION MEASURE FITS

Sequence number (1)	Source number (2)	log T_{max} (3)	log T^{+}_{max} (4)	log T^{-}_{max} (5)	α (6)	α^{+} (7)	α^{-} (8)	f_x 10^{13} erg s^{-1} cm^{-2} (9)	χ^2_{red} (10)	Xref number (11)
350	1	7.15	7.88	6.94	0.24	0.54	0.00	3.15	0.87	55
501	3	7.58	7.81	7.38	0.69	0.89	0.51	46.20	1.32	71
838	1	8.00	8.08	7.86	0.54	0.60	0.48	132.00	0.64	7
844	9	6.53	6.73	6.24	0.01	0.93	0.00	1.51	1.69	112
845	2	7.34	7.43	7.22	1.26	1.48	1.06	55.10	1.01	38
847	4	7.21	7.38	7.10	6.50	6.72	6.30	32.80	1.04	65
848	4	6.42	6.46	6.40	0.92	1.78	0.76	55.90	1.97	67
849	1	7.00	7.02	6.98	2.41	2.55	2.27	1170.00	2.01	61
865	3	7.62	7.73	7.50	0.71	0.83	0.59	46.10	0.56	49
905	7	8.03	8.14	7.85	0.27	0.35	0.19	28.60	1.62	1
906	3	8.00	8.11	7.77	0.23	0.35	0.12	36.30	0.52	1
907	1	7.58	7.66	7.53	0.88	0.96	0.80	130.00	1.61	8
908	3	7.79	7.85	7.66	0.83	0.91	0.75	92.20	2.20	8
917	4	7.58	7.70	7.50	0.87	0.99	0.77	38.30	2.20	13
927	1	7.51	7.55	7.47	0.98	1.04	0.92	151.00	1.11	18
933	1	7.84	7.92	7.72	0.41	0.47	0.35	105.00	0.95	24
2225	1	7.55	7.94	7.26	0.69	0.95	0.49	44.90	1.32	31
2300	2	7.35	7.51	7.26	4.10	4.84	3.68	55.10	0.58	36
2302	1	7.35	7.43	7.27	1.37	1.61	1.17	191.00	0.35	2
2306	1	7.78	7.81	7.73	1.63	1.75	1.53	1110.00	1.87	46
2308	1	7.31	7.37	7.26	1.26	1.46	1.14	157.00	1.27	7
2310	1	7.40	7.44	7.37	2.92	3.84	2.76	524.00	1.47	68
2311	1	7.58	7.62	7.53	1.79	1.93	1.61	422.00	0.94	68
2314	1	8.06	8.10	7.97	0.72	0.76	0.68	614.00	2.30	21
3048	6	7.61	7.67	7.52	0.51	0.55	0.47	62.60	1.56	8
3091	1	8.20	8.20	7.99	0.56	0.74	0.40	40.30	1.05	17
3106	1	7.36	7.50	7.24	0.39	0.49	0.29	124.00	2.02	44
3113	2	6.84	6.90	6.78	0.47	0.61	0.27	44.50	0.93	108
3192	1	8.20	8.20	8.10	1.33	1.49	1.21	502.00	1.36	35
3196	1	8.20	8.20	8.08	10.76	10.92	10.64	62.80	2.05	59
3208	2	7.42	7.52	7.35	5.41	6.67	4.51	155.00	1.04	82
3209	1	8.20	8.20	7.90	0.68	0.94	0.48	25.90	1.62	83
3211	3	8.20	8.30	8.04	1.63	2.31	1.31	118.00	1.09	85
3213	4	7.76	7.80	7.72	1.58	1.72	1.46	487.00	0.75	88
3219	1	7.39	7.43	7.35	1.91	2.07	1.77	573.00	1.08	100
3227	1	7.82	7.86	7.63	1.37	1.51	1.19	178.00	1.96	111
3229	1	8.20	8.20	7.65	3.21	3.47	2.69	33.30	2.39	117
3230	2	8.20	8.20	7.89	3.23	3.49	2.61	99.90	1.49	122
3231	3	8.20	8.20	8.02	10.60	10.86	9.98	41.60	2.34	124
3235	2	7.61	7.64	7.56	1.41	1.49	1.31	618.00	0.72	129
3236	1	7.96	8.02	7.89	1.44	1.58	1.26	359.00	1.33	130
3243	3	7.56	7.61	7.52	0.83	0.89	0.77	131.00	1.68	14
3365	4	7.54	7.57	7.51	1.29	1.37	1.23	101.00	1.27	29
3366	1	7.56	7.62	7.54	0.88	0.92	0.84	294.00	2.14	95
3512	2	8.20	9.16	7.72	0.37	0.55	0.19	38.60	0.81	52
3530	2	6.98	7.07	6.91	1.54	2.02	1.16	24.60	0.37	79
3531	2	7.05	7.14	6.95	0.82	1.04	0.62	39.00	1.32	87
3534	3	7.59	7.62	7.44	1.88	2.20	1.70	118.00	2.16	34
3535	1	7.45	7.55	7.39	1.84	2.50	1.68	136.00	0.95	75
3536	1	7.23	7.32	7.14	4.14	4.80	3.08	59.60	0.98	116
3720	5	7.58	7.76	7.41	1.10	1.34	0.90	8.40	0.99	63
3811	2	7.64	7.94	7.32	0.31	0.45	0.17	26.90	0.61	103
4347	2	7.49	7.61	7.32	0.46	0.58	0.34	71.40	0.39	64
4348	3	7.00	7.06	6.93	1.65	2.03	1.35	58.50	0.39	62
4414	2	7.30	7.62	7.13	0.37	0.53	0.21	16.00	0.83	9
4448	1	7.45	7.51	7.37	1.80	2.10	1.56	186.00	0.79	77
4452	4	7.13	7.18	7.07	2.29	2.67	2.01	150.00	1.58	33
4457	1	6.94	7.07	6.82	0.41	0.67	0.15	11.80	1.47	86
4496	1	7.77	7.79	7.70	1.71	1.81	1.59	1320.00	1.79	46
4942	3	7.20	7.34	7.08	6.13	6.59	5.79	12.50	1.10	57
5012	3	7.52	7.55	7.50	1.67	1.77	1.62	373.00	1.84	123
5013	3	7.48	7.51	7.45	1.54	1.62	1.44	328.00	2.20	123
5015	1	7.67	7.72	7.62	1.68	1.88	1.56	397.00	1.13	123
5016	1	7.82	7.85	7.68	1.29	1.41	1.19	279.00	2.22	123

TABLE 5—*Continued*

Sequence number (1)	Source number (2)	log T_{max} (3)	log T^{+}_{max} (4)	log T^{-}_{max} (5)	α (6)	α^{+} (7)	α^{-} (8)	f_x 10^{13} erg s^{-1} cm^{-2} (9)	χ^2_{red} (10)	Xref number (11)
5184	3	7.82	7.90	7.69	1.25	1.45	1.09	61.20	2.00	69
5185	4	7.76	7.84	7.27	0.29	0.49	0.09	9.51	0.77	73
5189	1	7.31	7.35	7.25	0.76	0.81	0.66	282.00	1.23	78
5190	2	7.23	7.29	7.12	1.79	2.23	1.53	52.90	1.61	80
5191	2	7.45	7.62	7.21	0.53	0.67	0.39	40.20	0.69	98
5448	4	6.97	7.04	6.86	1.29	1.63	0.99	39.90	0.98	41
5471	4	7.37	7.56	7.25	1.48	2.00	1.16	23.90	1.43	60
5484	2	7.39	7.57	7.29	0.77	0.89	0.61	63.90	1.16	4
5485	3	7.70	7.98	7.44	0.30	0.40	0.20	22.30	0.96	5
5493	4	7.03	7.17	6.91	1.20	1.68	0.86	10.90	1.30	6
5527	2	7.53	7.93	7.21	0.49	0.73	0.27	15.50	0.57	11
5538	2	6.98	7.11	6.85	0.41	0.69	0.19	10.80	1.40	81
5549	2	7.78	8.02	7.52	0.40	0.52	0.28	26.00	0.97	89
5559	7	7.21	7.24	7.15	1.34	1.56	1.26	91.80	1.03	91
5576	1	8.13	8.19	7.22	0.23	0.57	0.00	2.57	0.39	96
5584	4	7.22	7.41	7.05	3.27	3.61	2.83	10.80	1.69	101
5605	2	7.66	7.74	7.48	0.73	0.85	0.65	37.50	1.18	104
5621	2	6.98	7.04	6.94	1.60	1.78	1.38	18.50	0.46	110
5640	1	7.47	7.59	7.32	1.22	1.50	1.04	25.30	0.53	114
5645	4	7.42	7.51	7.28	1.22	1.50	1.06	27.80	1.70	115
5652	5	6.77	6.88	6.67	0.50	0.84	0.12	8.61	1.17	119
5990	1	7.44	7.54	7.31	0.81	0.94	0.71	54.30	1.31	12
5991	2	7.37	7.68	7.18	0.77	1.01	0.53	23.30	0.82	15
5992	2	7.00	7.20	6.84	0.41	0.73	0.13	8.02	2.30	102
5993	1	7.54	7.92	7.18	0.51	0.73	0.31	17.20	1.28	113
6080	4	7.75	7.98	7.33	0.29	0.47	0.11	9.14	0.78	37
6953	4	7.99	8.06	7.83	0.52	0.58	0.46	55.00	1.82	1
6964	6	7.02	7.05	6.99	1.19	1.29	1.09	41.30	1.80	71
6969	5	7.55	7.70	7.46	0.68	0.76	0.60	27.20	1.84	13
6972	1	7.80	7.85	7.76	0.79	0.85	0.75	240.00	0.95	24
6973	2	7.98	8.02	7.89	0.54	0.58	0.50	158.00	1.25	24
7359	1	7.45	7.72	7.21	0.80	1.10	0.56	34.80	0.52	3
7360	1	8.20	8.24	7.85	0.50	0.56	0.36	68.80	1.67	3
7361	1	7.40	7.54	7.29	1.15	1.39	0.97	79.50	0.91	3
7362	1	8.20	8.24	8.06	0.92	1.08	0.80	74.70	0.86	30
7363	2	7.93	8.08	7.72	0.52	0.62	0.42	40.80	0.98	30
7364	1	8.20	8.24	7.82	0.33	0.45	0.21	31.30	1.05	30
7380	2	7.87	7.94	7.74	0.52	0.58	0.46	254.00	1.04	23
7381	2	7.96	8.00	7.79	0.54	0.60	0.48	188.00	1.31	23
7382	1	8.20	8.24	7.98	0.40	0.44	0.30	152.00	0.70	23
7416	7	7.68	7.83	7.30	0.18	0.40	0.00	6.73	0.74	22
7471	2	8.11	8.26	7.93	0.70	0.84	0.58	38.10	0.89	27
7605	6	7.44	7.54	7.35	0.79	0.89	0.69	26.40	0.83	118
7606	2	7.91	8.07	7.70	0.42	0.50	0.34	25.20	1.65	48
7607	4	7.24	7.38	7.08	2.35	3.49	1.63	30.80	0.66	76
7609	4	7.14	7.19	7.09	2.53	3.13	2.13	44.60	0.47	97
7610	3	7.18	7.29	7.11	4.53	5.13	4.07	14.30	1.40	99
7611	6	7.03	7.10	6.96	2.80	4.14	2.18	6.19	1.15	106
7663	1	7.07	7.28	6.90	0.42	0.70	0.16	17.20	1.19	103
7710	2	8.01	8.03	7.66	0.50	0.68	0.34	16.50	0.28	25
7737	4	8.20	8.24	8.03	1.10	1.38	0.88	71.00	1.21	40
7749	5	7.25	7.33	7.19	1.14	1.34	1.04	40.30	2.00	28
7888	4	6.95	7.04	6.85	0.81	1.09	0.53	17.90	0.95	105
7913	2	6.84	6.90	6.80	2.81	3.91	2.41	28.10	1.43	84
7918	6	6.94	7.04	6.85	0.82	1.08	0.58	13.40	0.23	47
7954	4	7.15	7.42	6.99	0.31	0.51	0.11	7.23	0.64	74
7958	6	7.36	7.54	7.13	0.45	0.63	0.27	8.34	1.23	32
8396	7	7.21	7.27	7.17	6.93	7.13	5.73	39.20	1.12	128
9002	5	7.33	7.58	7.19	0.76	0.94	0.60	10.50	0.90	50
9004	6	7.40	7.45	7.34	1.21	1.31	1.11	50.90	1.52	51
9005	5	7.02	7.13	6.99	1.45	1.63	1.31	23.30	1.46	52
9005	9	7.36	7.66	7.12	0.82	1.12	0.56	6.61	0.50	53
9006	7	7.31	7.52	7.22	1.07	1.29	0.89	11.30	1.52	54
9041	1	7.79	7.83	7.77	1.56	1.66	1.48	1280.00	0.92	43
9065	3	7.46	7.60	7.32	0.51	0.63	0.41	45.50	1.10	42
9692	3	7.01	7.11	6.97	1.13	1.31	0.97	27.40	1.76	66

TABLE 5—*Continued*

Sequence number (1)	Source number (2)	log T_{max} (3)	log T^{+}_{max} (4)	log T^{-}_{max} (5)	α (6)	α^{+} (7)	α^{-} (8)	f_x 10^{13} erg s^{-1} cm^{-2} (9)	χ^2_{red} (10)	Xref number (11)
9705	1	7.01	7.19	6.91	1.54	2.12	1.16	12.40	0.59	90
9711	1	7.37	7.72	7.09	0.81	1.13	0.55	10.80	1.34	121
9967	1	7.76	7.82	7.74	1.48	1.58	1.40	789.00	2.30	43
10100	2	6.84	6.94	6.77	2.15	3.71	1.77	10.50	0.80	70
10311	2	7.97	8.18	7.80	0.29	0.37	0.21	46.30	0.83	19
10312	2	7.45	7.57	7.38	0.77	0.85	0.69	43.60	1.18	20
10418	1	7.37	7.49	7.31	0.70	0.78	0.62	152.00	1.38	94
10538	8	7.12	7.24	7.06	5.03	5.07	4.59	21.50	2.19	56
10640	2	7.47	7.53	7.42	1.01	1.09	0.95	114.00	1.07	8

"g" and "r," respectively. Main-sequence stars with $B-V < 1$ appear largely in the low-α region of the graph (with a few exceptions), while K and M dwarfs are confined to the low α–high T_{max} region. Giants tend to have high values of α and intermediate values of T_{max}, while RS CVn systems are characterized by very high temperatures and relatively high α values. The derived values of α are seen to be largest for temperatures around log $T_{max} \sim 7.2$ and $T_{max} = 8.2$, the latter value arising (at least partially) because it is the upper boundary of the temperature grid employed. Note also that the two objects with lowest values of T_{max} represent the nearby stars Procyon (F5 V–IV) and Altair (A7 V).

d) Stars with No Acceptable Coronal Model

For eight observations (of seven sample stars: [1], [10], [16], [46], [92], [93], and [109]), we were unable to find any spectral model (within the range of parameters considered) that produced an acceptable fit to their measured IPC spectra. The final column of Table 1 indicates this condition with the letter "U." (Other "fit codes" appearing in Table 1 are defined in Table 6.)

A fit can be unsuccessful because the minimum value of χ^2_{red} exceeds our threshold of 2.5, because no reasonable constraints in the fit parameters could be derived, or because the formal minimum obtains for unphysical values of the parameters (as occurred for the fixed two-temperature model in a total of 30 observations denoted with fit codes containing "−" in Tables 1 and 6). Inspection of Table 1 reveals that four failures to derive acceptable models were due to observations with large signal-to-noise ratio; had we included systematic errors in the χ^2 calculation (see Appendix B), we believe that formally acceptable fits would have been obtained (i.e., these failures stem from the fact that the systematic errors dominate the statistical errors for such high signal-to-noise-ratio observations). The remaining four cases were just marginally above our cutoff level in χ^2_{red}, and we therefore argue that virtually all IPC spectra of nearby stars can be fitted with simple, thermal-emission models. (The fact that three other observations of one of these stars [1] produced acceptable fits supports this contention.)

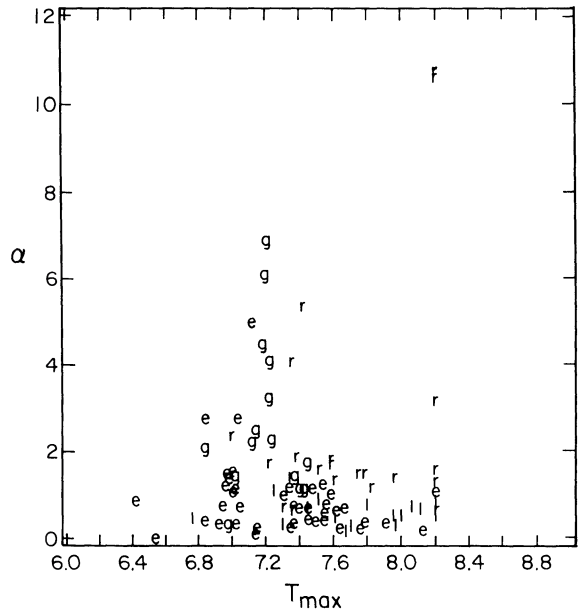

FIG. 10.—Scatter plot of α vs. T_{max} for successful continuous emission measure fits. Different plotting symbols denote the following: g = giants; r = RS CVn stars; e = main-sequence stars with $B-V < 1$; and l = main-sequence stars with $B-V > 1$.

TABLE 6

SUMMARY OF MODEL-FITTING RESULTS

Table 1 Fit Code	Number of Observations	Comments	Number of Stars
A	61	All models fit	51
A−	17	EM unphysical	13
A+	15	EM fails	12
12E	1	CONT fails	0
12	1	1T and 2T fit	0
12−	3	1T and 2T fit (EM unphysical)	1
1−	10	Only 1T fits (EM unphysical)	8
1	1	Only 1T fits	0
2EC	34	1T fails	18
2C	12	2T and CONT fit	5
2	2	Only 2T fits	1
U	8	All models fail	5
.....		Stars with multiple observations giving different results	16
Total	165	...	130

V. CONCLUSIONS

We have carried out a survey of coronal temperatures of late-type stars included in the Bright Star Catalog, its Supplement, and/or the Woolley Catalog and whose observations with the *Einstein* IPC were sufficiently long to produce X-ray spectra containing at least 200 counts.

An important step in the interpretation of the spectral fits is a detailed study of how the coronal parameters are derived from low spectral resolution data. We demonstrate by simulation (cf. Appendix C) that, given X-ray spectra of sufficiently high signal-to-noise ratio, the IPC is capable of reproducing simple coronal emission models. Furthermore, the large number of analyzed observations and resulting spectral fits enable us to study systematic effects of our fitting procedure with regard to the number of counts in the spectrum; this procedure is essential if we are to have confidence in our interpretation of the physical characteristics of the objects under study.

Thus, we find that IPC spectra containing fewer than ~ 500 counts can always be described adequately with a single-temperature model. X-ray spectra containing more than ~ 1000 counts show an interesting dichotomy, which is surely not an artifact of our analysis, but must represent an intrinsic property of the coronal spectra. Late-type main-sequence stars (usually of spectral type M) always exhibit both a high- and a low-temperature component, with the emission measure of the high-temperature component substantially larger than that of the low-temperature component; in essentially all cases, there is evidence for plasma at temperatures in excess of 10^7 K. On the other hand, most main-sequence stars of earlier type (i.e., spectral type F or G) do not show this high-temperature component and are instead dominated by plasma at lower temperature. In fact, from the X-ray point of view they appear very much like the Sun in full disk observations (in the absence of strong flares). We note in this context that the high-temperature plasmas that we observe do not appear to be directly associated with obvious flares, i.e., they are found during periods of "quiescent" emission when no variability is apparent.

In contrast to the main-sequence stars, yellow giants of our sample do show a high-temperature component which is not accompanied by low-temperature emission. The lack of this soft component seems to be an intrinsic property of these objects and is not caused by absorption of a soft component by the interstellar medium. However, since giant stars in the low-luminosity tail of the X-ray luminosity function are too weak to meet our criterion for counts in the X-ray spectrum, we cannot extend this result to the those members of this class.

We demonstrate that two-temperature models must be carefully interpreted. For models with true bimodal temperature distributions, we show that our IPC procedures faithfully reproduce the temperatures and emission measures of the simulated model stars. However, for models with continuous emission measure distributions as a function of temperature, our two-temperature analysis leads to a rather pronounced clustering of the temperature components at $\log T = 6.4$ and $\log T = 7.2$; this clustering is the result of an instrument-dependent, weighted averaging of the detected flux, an interpretation consistent with earlier studies of such source analyses (in a solar context) by Underwood and McKenzie (1977). In this respect, X-ray temperatures derived from low-resolution data such as the IPC spectra for one and two-temperature models should more properly be regarded as effective temperatures, and not as physical temperatures of the observed plasma.

In an attempt to characterize our X-ray spectra in a more physical, and less instrument-affected manner, we have considered differential emission measure distributions of the simple analytical form, $Q(T) \sim T^{\alpha}$. Distributions of such form arise naturally in plasmas whose energy balance is determined through heat conduction and radiation; in the simple case of a magnetic loop with constant pressure, heating rate, and cross section, the power-law coefficient α can be related to the radiative cooling rate $P(T)$. While such emission measure distributions should apply only to individual features in a stellar corona, but not necessarily to the overall X-ray spectrum, such distributions provide a useful starting point for a physically oriented interpretation of the X-ray spectra. This point of view is supported by *EXOSAT* transmission grating data available for Capella and σ CrB, which allow a full differential emission measure analysis (Mewe *et al.* 1986) and are not in conflict with an overall increasing emission measure distribution with temperature.

Application of the continuous emission measure model produces acceptable fits in a large number of cases for which a single-temperature description fails and a two-temperature description is otherwise required. An interesting result of this analysis is that temperatures significantly larger than those obtained from a straightforward one- or two-temperature analysis may in fact be present in many stellar coronae, particularly in active M-type dwarf stars. For main-sequence stars, the values of the power-law slope α cluster near unity, consistent with solar-type loops (i.e., loops with constant cross section) being responsible for the X-ray emission. For giant stars, on the other hand, we require values of α larger than unity in order to obtain acceptable fits; this is of course consistent with our earlier finding that single-temperature fits (with high temperatures, well in excess of 10^7 K) suffice to provide acceptable fits. Finally, RS CVn systems systematically show higher temperatures than any of the other types of stars and, as is the case for giants, slopes α larger than unity. Therefore we are ultimately led to the conclusion that the differential emission measure distributions in main-sequence F and G stars, main sequence M stars, yellow giants, and RS CVn systems are intrinsically different.

We would like to thank S. Saar for his careful reading of the manuscript and for calling our attention to the useful catalog of Strassmeier *et al.* (1988). One of us (J. H. M. M. S.) acknowledges the support of the Max-Planck-Gesellschaft. G. S. V. wishes to thank the Italian IAIF-CNR for support. This work was supported in part by the Italian Ministry for Public Education, by the Italian National Research Council (GNA), by the Italian Space Agency (ASI), and by NASA contract NAS8-30751.

APPENDIX A

THE INSTRUMENT

In this paper we present results obtained with the *Einstein Observatory* IPC, which was sensitive in the passband $\sim$0.15–4 keV, with an energy resolution of $\Delta E/E \sim 1$ at 1 keV, and two rather pronounced peaks in its effective area, at 0.28 keV (i.e., just below the carbon edge) and at $\sim$1.5 keV. Because the IPC was a proportional counter with many individual anode wires, the observed spectra were subject to spatial gain variations, and a knowledge of the detector gain at the position of the detected X-ray source is required when accurate spectral analysis is performed. The so-called IPC REV-1 processing system (cf. Harnden *et al.* 1984) provides the necessary information in the form of gain histograms for objects detected in the center of the field of view, where the gain information is quite precise (the vast majority of the X-ray spectra discussed here). In also using some off-axis data, we have introduced somewhat larger uncertainties in the fitted parameters, because the gain calibration was less precise off axis, but since we are primarily interested in statistical ensembles (and not single objects) we are able to tolerate that increased uncertainty (for a further discussion of the effects of gain on fitted parameters, see Schmitt *et al.* 1985*b*).

For the spectral analysis we used all counts collected in a 3′ radius circle about the maximum likelihood position of the X-ray source and determined the background from the counts in an annulus with radii of 5′ and 6′. All sources detected near the entrance-window support structure or field-of-view edges were removed from our sample. The net number of counts in each pulse height channel was then compared, via the χ^2 statistic (cf. Appendix B), to the number predicted by convolving the various models with the IPC response.

APPENDIX B

FITTING PROCEDURES

The coronal models considered by us are discussed in § III*b* and can all be parameterized with a few physically interpretable parameters. In the simplest case, i.e., that of a single-component, isothermal plasma, the theoretically computed spectrum can be parameterized by an emission measure EM (i.e., a normalization constant) and a temperature T. By folding the computed spectrum with the detector response matrix, the expected number of counts in the ith detector channel $n_{i,\mathrm{ex}}(T, \mathrm{EM})$ is obtained. The best-fit spectrum, and hence EM and T, follow from minimizing the χ^2 test statistic defined through

$$\chi^2 = \sum_{i=1}^{N} \frac{(n_{i,\mathrm{obs}} - n_{i,\mathrm{ex}}(T, \mathrm{EM}))^2}{(\sigma_i)^2}, \tag{B1}$$

where N denotes the total number of detector channels and σ_i the error in the observed number of counts $n_{i,\mathrm{obs}}$ in the ith channel. Since two parameters, EM and T, are to be derived from the data, the test statistic

$$\chi^2_{\mathrm{red}} = \frac{\chi^2}{N-2} \tag{B2}$$

will be distributed like a χ^2 distribution with $N-2$ degrees of freedom.

The process of "folding" the incident spectrum with the detector response matrix involves another source of error, i.e., errors in the instrument calibration (effective areas) which are not known with great precision. In the case of thermal line spectra, the problem is aggravated by the fact that the effective areas at only a few selected energies, i.e., the energies of the strongest lines in the spectrum, matter. Sometimes systematic errors are included into the error budget by adding some fraction of $n_{i,\mathrm{obs}}$ to the statistical error σ_i; however, we decided to refrain from such more or less ad hoc procedures. As a consequence, for strong sources our error estimates are too optimistic and the derived values of χ^2 too large. We note in passing that we derive errors only for the estimated temperatures, while the normalization constants (which determine the derived emission measures) are treated as "uninteresting parameters" in our error budget.

Further, the test statistic (B1) may have more than one minimum; this may in particular happen when nonzero values of N_{H} are considered. While only one global minimum is likely to exist, any numerical, minimum-finding algorithm can easily be trapped in a local minimum. In order to avoid such difficulties we performed an initial grid search over the interesting parameter space to find a suitable starting point for the minimization algorithm. Clearly, such a procedure is not guaranteed to find a global minimum unless an unreasonably fine grid is chosen to start with; however, we believe that the minima presented in our paper represent in fact the global minima for the models considered.

APPENDIX C

SPECTRAL SIMULATIONS

In order to convince ourselves of the capability of the IPC to determine coronal parameters, we performed an extensive series of spectral fits to simulated IPC spectra derived from known input spectra. Such simulations are by definition free of any systematic errors and allow us to ascertain the quality of our fit results as a function of signal-to-noise ratio.

a) One- and Two-Temperature Models

Fitting the observed pulse height distribution to one- or two-temperature models is the most common procedure to analyze thermal X-ray spectra. It is computationally straightforward, and leads—with two components—to a satisfactory statistical description of most coronal IPC X-ray spectra. However, as a first step, we demonstrate the capability of the IPC to retrieve an isothermal (i.e., single-component) spectrum in a low signal-to-noise ratio situation. As an input, we chose a temperature of log $T = 6.8$, which is actually right in the "gap" of "forbidden" X-ray temperatures (cf. Fig. 8), and fold the resulting incident spectrum through the IPC. In Figure 11 we show a histogram of derived X-ray temperature (obtained via a χ^2 fit to the synthetic IPC spectrum). While this distribution is broad—because of the small number of counts in the incident simulated spectrum—the peak of the distribution does occur at the correct input temperature, thus demonstrating that the temperatures of isothermal coronae could be inferred with the IPC if isothermal coronae existed in nature, even when the coronal temperatures fall in the gap of "forbidden" X-ray temperatures.

For observations with higher signal-to-noise ratio, the single-component model usually proves to be inadequate, and one therefore proceeds to more complex models. For incident X-ray spectra containing 10,000 counts, based on a coronal model consisting of two temperature components at log $T = 6.4$ and log $T = 6.9$ and an emission measure ratio of 4, Figure 12 shows the X-ray temperatures inferred by fitting the synthetic spectra. As before, the histogram peaks quite sharply at the correct high temperature, but the distribution is more broadly peaked at lower temperatures, both because the rather small emission measure in the low-temperature component leads to a relatively lower effective signal-to-noise ratio for this component, and because the spectral resolution of the IPC is limited. This case is in fact a "worst case" in that the higher temperature component again falls into the "forbidden" temperature domain for the IPC, whereas the observed sources tend to have a substantially higher value for the high-temperature component. Figure 12 shows that even in this case, the two components can be correctly inferred.

As an aside, we note that if the incident spectrum is produced by a truly heterothermal plasma, further complications may arise. For example, Underwood and McKenzie (1977) studied X-ray filtergrams obtained with the S-056 *Skylab* instrument, showing that derived X-ray temperatures depend on the specific filter pair used if line-of-sight temperature gradients are present, i.e., the derived temperatures were a weighted mean of the observed plasma's temperatures, where the weighting function is determined by the instrument's characteristics. (Note that temperature determination from a filter ratio is just a special case of eq. [B1] with $N = 2$ and no degrees of freedom.) If stellar coronae are indeed similar to the Sun's corona (which is known to be intrinsically heterothermal, with a variety of "temperature components" present along any given line-of-sight), then the complete lack of spatial resolution in the stellar observations aggravates the problem even further: at any given time, the entire corona is visible except for those parts blocked by the stellar disk. Under these circumstances, one must be aware that the derived temperatures need not necessarily have an immediate physical interpretation, and any isothermal model accounting for the harder energy channels will underpredict the count rate in the softer energy channels. In order to fit the overall spectrum, a second component must be introduced at a temperature where the IPC is still reasonably sensitive, and where the harder energy channels are least affected. This "juggling" of the two component temperatures is thus strongly affected by the precise nature of the detector's spectral response, and therefore the location of the two fit temperatures may not directly describe a physical property of the X-ray emitting plasma.

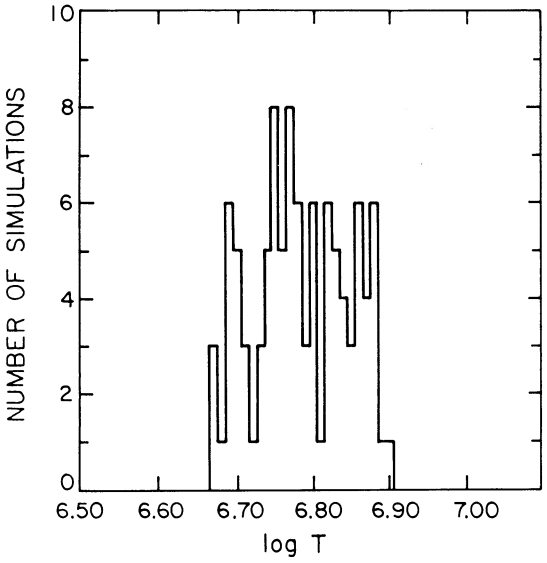

FIG. 11

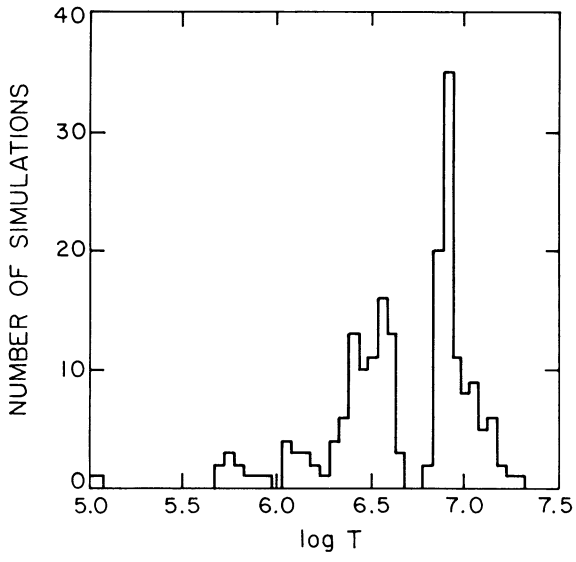

FIG. 12

FIG. 11.—Frequency of occurrence of log T values inferred from single-temperature model fits to simulated IPC spectra. Note that the analysis correctly infers (in a statistical sense) the temperature of log $T = 6.8$ used to simulate the thermal plasma spectra with 500 counts.

FIG. 12.—Frequency of occurrence of log T values inferred from two-temperature model fits to simulated spectra containing 10,000 counts; temperature components for the simulations were chosen at log $T = 6.4$ and log $T = 6.9$, with an emission measure ratio 1:4. Note that the lower temperature component is much less constrained than the higher component.

b) Continuous Emission Measure Models

We next consider continuous emission measure distributions, and demonstrate that the IPC can also reproduce such models. Most of the solar X-ray emission appears to be emitted by loop structures (Vaiana and Rosner 1978), and in the simplest case, the temperature stratification in individual loops is determined by a balance between heating, conduction and radiation (see, for example, Rosner, Tucker and Vaiana 1978); differential emission measure distributions, i.e., models with many "temperature components" present, naturally arise in this way. For the Sun, the theoretically computed differential emission measure distributions for loops agree rather well with the observations at high temperature, whereas at lower temperatures, discrepancies appear whose cause is not entirely clear (and which are of no consequence in the present discussion).

For our simulations we assumed a continuous emission measure distribution with log $T_{max} = 7.5$ and power-law slope $\alpha = 1.2$; in Figure 13 we show the values of α and T_{max} obtained by fitting 100 random realizations of the same spectrum, based on the assumed differential emission measure distribution (each realization containing about 10,000 counts). While the spread in the derived values of α and T_{max} is rather large, and the derived parameters are correlated, with a tendency for large slopes to go with lower maximum temperatures and vice versa, the simulations also show that on average the correct parameters can be retrieved. It turns out that the same spectra can also be successfully fitted with a two-temperature model (cf. Schmitt *et al.* 1987), while a one-temperature description fails to fit in essentially all realizations.

In order to understand whether the large values of α found around $T_{max} = 7.2$ (cf. Fig. 9*b*) are real or rather an artifact of the instrument, we also performed a set of simulations with signal-to-noise ratio representative of the majority of real data. In particular, we simulated spectra with 500 counts, $T_{max} = 7.2$ and with emission measure slopes $\alpha = 0.0, 1.0, 2.0, 4.0$; for each value of α, 20 realizations were generated and fitted. The results of the continuous emission measure fits of these simulated spectra are shown in Figure 14; crosses denote input values $\alpha = 0$, upward-pointing triangles $\alpha = 1$, downward-pointing trianges $\alpha = 2$, squares $\alpha = 3$, and diamonds $\alpha = 4$. We find that for input α values between 0 and 1, the correct α are values reproduced, while for input values $\alpha > 1$ the retrieved α's tend to be larger than the input ones; we also note the increase of spread in the inferred temperatures toward lower values of α. For our interpretation of real data, it is relevant to note that inferred values of α much larger than unity at $T_{max} \sim 7.2$ are presumably indicative of an actual slope of the emission measure distribution >1 (although they may be an overestimate of the real slope), and that inferred temperatures in spectra with α close to (or lower than) unity are affected by large errors (see next paragraph for comments on this effect).

Last, we performed high signal-to-noise ratio spectral simulations of continuous emission measure distributions with a wide range of maximum temperatures (log $T_{max} = 6.5, 7.0, 7.5$) and emission measure slopes ($\alpha = 0.0, 2.0, 4.0$) in order to explore the full range of parameters found in our IPC spectra. For each choice of parameters, 20 random realizations with a total number of 5000 counts were obtained and a continuous emission measure analysis performed; the results are shown in Figure 15. From Figure 15 it becomes clear that, at least in the high signal-to-noise ratio cases, the IPC can reliably reconstruct the model parameters over a wide range of temperatures T_{max} and emission measure slopes α. However, for larger values of temperature and slope, especially the inferred slopes have a rather large scatter; note that in this case the incident spectra are not far from those of an isothermal plasma. For the case of almost flat emission measure distributions, the maximum temperatures cannot be determined very well, clearly an

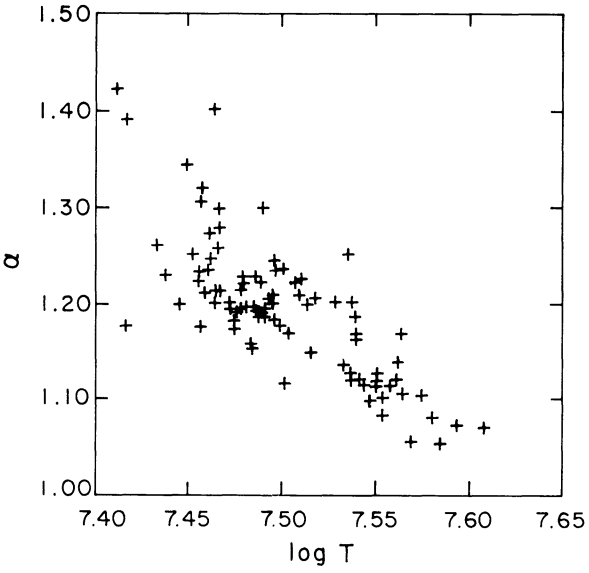

FIG. 13

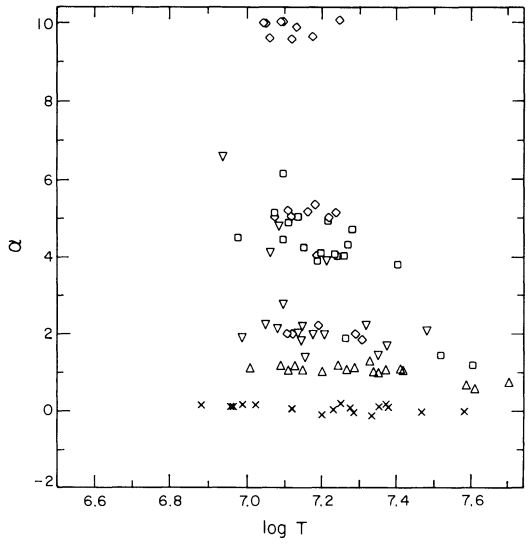

FIG. 14

FIG. 13.—Plot of α vs. T_{max} for IPC spectral simulations of continuous emission measure distributions; input spectra contained 10,000 counts and took the differential emission measure distribution as $Q(T) \sim T^{\alpha}$ for $T < T_{max}$, with log $T_{max} = 7.5$ and $\alpha = 1.2$. Note how well the input emission distribution is statistically inferred.

FIG. 14.—Plot of α vs. T_{max} for IPC spectral simulations of continuous emission measure distributions with log $T_{max} = 7.2$ and $\alpha = 0.0$, 1.0, 2.0 and 4.0. Input spectra containing 500 counts with a differential emission measure distribution $Q(T) \sim T^{\alpha}$ for $T < T_{max}$ were chosen. Although large values of α tend to be overestimated, values of α around unity are correctly inferred (see text).

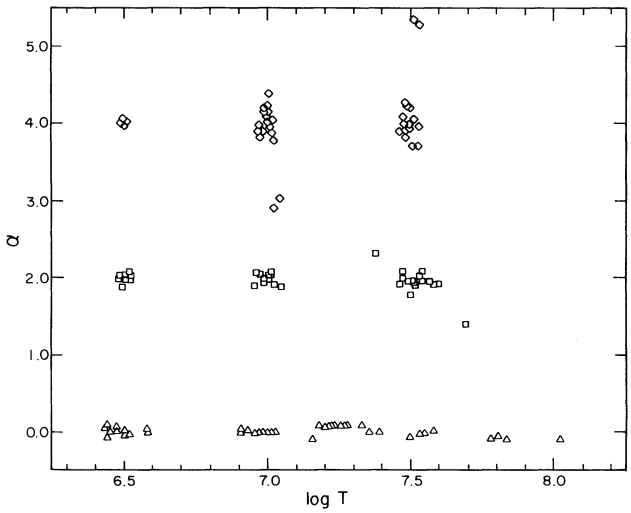

FIG. 15.—Plot of α vs. T_{max} inferred from simulated IPC spectra of continuous emission measure distributions with log T_{max} = 6.5, 7.0, 7.5 and α = 0.0, 2.0, and 4.0. Input spectra with 5000 counts were generated using a differential emission measure distribution $Q(T) \sim T^{\alpha}$ for $T < T_{max}$. Note how well the input emission distribution is statistically inferred as long as the values of slope and maximum temperature do not become too large. See text for details, including a description of the symbols which follow those of Fig. 14.

instrumental effect since only a small fraction of the recorded counts is produced by the very highest temperatures (to which the IPC was not particularly sensitive).

REFERENCES

Agrawal, P. C., Markert, T. H., and Riegler, G. R. 1985, *M.N.R.A.S.*, **213**, 761.
Antiochos, S. K., and Noci, G. 1986, *Ap. J.*, **301**, 440.
Ayres, T. R., Linsky, J. L., Vaiana, G. S., Golub, L., and Rosner, R. 1981, *Ap. J.*, **200**, 293.
Gaetz, T. J., and Salpeter, E. E. 1983, *Ap. J. Suppl.*, **52**, 155.
Chambers, J. M., Cleveland, W. S., Kleiner, B., and Tukey, P. A. 1983, *Graphical Methods for Data Analysis* (Belmont, Ca.: Wadsworth).
Giacconi, R., *et al.* 1979, *Ap. J.*, **230**, 540.
Gondoin, P., Mangenay, A., and Praderie, F. 1987, *Astr. Ap.*, **174**, 187.
Gorenstein, P., Harnden, F. R., Jr., and Fabricant, D. G. 1981, *I.E.E.E. Trans. Nucl. Sci.*, **NS-28**, 869.
Haisch, B. M. 1987, in *Cool Stars, Stellar Systems, and the Sun* (Berlin: Springer), p. 269.
Haisch, B. M., and Simon, T. 1982, *Ap. J.*, **263**, 252.
Harnden, F. R., Jr., Fabricant, D. G., Harris, D. E., and Schwarz, J. 1984, *Smithsonian Ap. Obs. Spec. Rept.*, No. 393.
Hoffleit, D., and Jaschek, C. 1982, *The Bright Star Catalog* (4th rev. ed.; New Haven: Yale University Press) (BSC).
Hoffleit, D., Saladyga, M., and Wlasuk, P. 1984, *Supplement to The Bright Star Catalog* (New Haven: Yale University Press).
Kato, T. 1976, *Ap. J. Suppl.*, **30**, 397.
Landini, M., and Monsignori-Fossi, B. C. 1970, *Astr. Ap.*, **6**, 468.
———. 1984, *Phys. Scripta*, **T7**, 53.
Linsky, J. L. 1985, *Solar Phys.*, **100**, 333.
Maggio, A., *et al.* 1987, *Ap. J.*, **315**, 687.
Maggio, A., Vaiana, G. S., Haisch, B., Stern, R., Bookbinder, J., Harnden, F. R., Jr., and Rosner, R. 1990, *Ap. J.*, **348**, 253.
Majer, P., Schmitt, J. H. M. M., Golub, L., Harnden, F. R., Jr., and Rosner, R. 1986, *Ap. J.*, **300**, 360.
Mewe, R. 1972, *Astr. Ap.*, **20**, 215.
Mewe, R., *et al.* 1982, *Ap. J.*, **260**, 233.
Mewe, R., Gronenschild, E. H. B. M., and van den Oord, G. H. J. 1985, *Astr. Ap. Suppl.*, **152**, 446.
Mewe, R., Schrijver, C. J., Lemen, J. R., and Bentley, R. D. 1986, *Adv. Space Res.*, Vol. **6**, No. 8, p. 133.
Micela, G., *et al.* 1985, *Ap. J.*, **292**, 172.
Micela, G., Sciortino, S., Vaiana, G. S., Harnden, F. R., Jr., Rosner, R., and Schmitt, J. H. M. M. 1990, *Ap. J.*, **348**, 557.
Micela, G., Sciortino, S., Vaiana, G. S., Schmitt, J. H. M. M., Stern, R. A., Harnden, F. R., Jr., and Rosner, R. 1988, *Ap. J.*, **235**, 798.
Pettersen, B. R. 1982, in *IAU Colloquium 71, Activity in Red Dwarf Stars*, ed. P. R. Byrne and M. Rodonò (Dordrecht: Reidel), p. 17.
Raymond, J. C. 1985, private communication.
———. 1988, *Hot Thin Plasmas in Astrophysics*, ed. R. Pallavicini (Dordrecht: Kluwer), p. 3.
Raymond, J. C., and Smith, B. W. 1977, *Ap. J. Suppl.*, **35**, 419.
Rosner, R., Golub, L., and Vaiana, G. S. 1985, *Ann. Rev. Astr. Ap.*, **23**, 413.
Rosner, R., Tucker, W. H., and Vaiana, G. S. 1978, *Ap. J.*, **220**, 643.
Rosner, R., *et al.* 1981, *Ap. J. (Letters)*, **249**, L5.
Schmitt, J. H. M. M. 1984, in *X-ray Astronomy 84*, ed. M. Oda and R. Giacconi (Bologna: ISAS), p. 17.
Schmitt, J. H. M. M., Golub, L., Harnden, F. R., Jr., Maxson, C. W., Rosner, R., and Vaiana, G. S. 1985*a*, *Ap. J.*, **290**, 307.
Schmitt, J. H. M. M., Harnden, F. R., Jr., Peres, G., Rosner, R., and Serio, S. 1985*b*, *Ap. J.*, **288**, 751.
Schmitt, J. H. M. M., Pallavicini, R., Monsignori-Fossi, B. C., and Harnden, F. R., Jr. 1987, *Astr. Ap.*, **179**, 193.
Schrijver, C. J. 1985, *Space Sci. Rev.*, **40**, 3.
Shull, J. M. 1981, *Ap. J. Suppl.*, **46**, 27.
Stern, R. A., Antiochos, S. K., and Harnden, F. R., Jr. 1986, *Ap. J.*, **305**, 417.
Strassmeier, K. G., Hall, D. S., Zeilik, M., Nelson, E., Eker, Z., and Fekel, F. C. 1988, *Astr. Ap. Suppl.*, **72**, 291.
Swank, J. H. 1984, in *The Origin of Nonradiative Heating/Momentum in Hot Stars*, ed. A. B. Underhill and A. G. Michalitsianos (NASA Conference Publication 2358), p. 86.
Tucker, W. H., and Koren, M. 1971, *Ap. J.*, **168**, 283.
Tukey, J. W. 1977, *Exploratory Data Analysis* (Reading, Mass.: Addison-Wesley).
Underwood, J. H., and McKenzie, D. L. 1977, *Solar Phys.*, **53**, 417.
Vaiana, G. S. 1983, in *IAU Symposium 102, Solar and Stellar Magnetic Fields: Origins and Coronal Effects*, ed. J. O. Stenflo (Dordrecht: Reidel), p. 165.
Vaiana, G. S., and Rosner, R. 1978, *Ann. Rev. Astr. Ap.*, **16**, 393.
Vaiana, G. S., *et al.* 1981, *Ap. J.*, **245**, 163.
Vedder, P. W., and Canizares, C. R. 1983, *Ap. J.*, **270**, 666.
Woolley, R., *et al.* 1970, *Royal Obs. Ann.*, **5**.

A. COLLURA, S. SCIORTINO, and G. S. VAIANA: Osservatorio Astronomico di Palermo, Palazzo dei Normanni 1, 90134 Palermo, Italy

F. R. HARNDEN, JR.: Harvard-Smithsonian Center for Astrophysics, 60 Garden Street, Cambridge, MA 02138

R. ROSNER: Department of Astronomy and Astrophysics, and Enrico Fermi Institute, The University of Chicago, 5640 South Ellis Avenue, Chicago, IL 60637

J. H. M. M. SCHMITT: Max-Planck-Institut für Extraterrestrische Physik, D-8046 Garching bei München, Germany